OL | Organic Letters

pubs.acs.org/OrgLett Letter

Perhalogenated Tetraazaperopyrenes and Their Corresponding Mono- and Dianions

Benjamin A. R. Günther, Sebastian Höfener, Robert Eichelmann, Ute Zschieschang, Hubert Wadepohl, Hagen Klauk, and Lutz H. Gade*

Cite This: *Org. Lett.* 2020, 22, 2298–2302 Read Online

ACCESS | Metrics & More | Article Recommendations | Supporting Information

ABSTRACT: Chlorination and bromination of 2,9-perfluoropropyl-substituted tetraazaperopyrenes (TAPPs) under forcing conditions resulted in fully core-halogenated TAPP derivatives, devoid of hydrogen atoms at the polycyclic aromatic core. The octahalogenation stabilized the reduced mono- and dianionic compounds sufficiently to allow for their characterization. The additional ortho-chlorination led to an improvement of the electron mobility compared to the bay-substituted tetrachloro-TAPP when employed as an n-channel semiconductor in thin-film transistors.

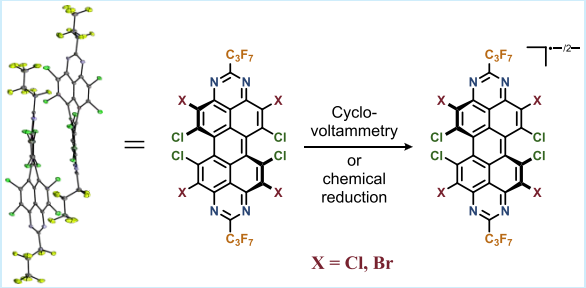

The design and synthesis of organic materials with electron-accepting properties which perform satisfactorily as electron (n-channel) semiconductors remains a challenging task.[1−6] Promising strategies are based on the isosteric CH → N-substitution within the organic framework[7−9] and the introduction of electron-withdrawing groups,[10−12] which both lead to significant stabilization of frontier orbitals. Low-lying lowest unoccupied molecular orbitals (LUMOs) in particular are a prerequisite for the application as n-channel semiconductors by decreasing the electron-injection barrier at the interface between the active layer and the electrodes.[13,14] Additionally, they stabilize the reduced species, making it even possible to isolate and characterize these under certain conditions.[15−24]

A class of compounds that has received particular attention in this context is the group of perylene diimides (PDIs). Facile modification of the perylene core[25] allows the precise adjustment of electronic properties leading to manifold applications, e.g. in biomolecular imaging[26,27] or as electron acceptors in organic photovoltaics[3,28] and thin-film transistors (TFTs).[12,29,30] However, relatively few examples of fully core-substituted species have been reported,[22,24,31−35] as the typical modification is constrained to substitution at the bay- or imide-positions. A related electron-deficient class of polycyclic aromatic hydrocarbons (PAHs) with considerable potential as redox-active functional materials are tetraazaperopyrenes (TAPPs).[36] Albeit less studied than PDIs, applications as fluorescence markers in biological systems[37,38] or n-channel semiconductors for organic TFTs have been reported recently.[39−42]

The substitution at the 2,9-positions[43] and the core-functionalization at the ortho-positions[39−42,44] are well established. Furthermore, we recently developed an alternative synthesis that provides access to nonplanar TAPP derivatives by bay-substitution.[45]

Following on from the synthesis of bay-chlorinated TAPP derivatives (represented here by the 2,9-perfluoroalkyl-substituted **I**), we report the subsequent functionalization resulting in fully core-halogenated TAPP derivatives, devoid of hydrogen atoms at the polycyclic aromatic core. The principal challenge proved to be the deactivation of the ortho-positions[39,40] for the bay-chlorinated TAPP toward electrophilic substitution, due to the decreased electron density within the aromatic core compared to the nonfunctionalized parent compound.

For the ortho-halogenation of TAPP derivative **I**, the reaction conditions had to be modified, as no reactivity was observed under the previously established halogenation conditions. To achieve full chlorination of the TAPP core to generate compound **1**, the use of chlorosulfonic acid was essential (Scheme 1), while fourfold ortho-bromination was achieved only after reaction at 120 °C for 7 days to afford compound **2**. The perfluoroalkyl groups in the 2,9-positions of the starting material were found to be necessary to stabilize the compounds under the applied harsh reaction conditions.

Single crystal X-ray diffraction of both perhalogenated TAPPs **1c** and **2** confirmed the expected twist of the peropyrene core (denoted δ), observed previously for

Received: February 7, 2020
Published: March 2, 2020

https://dx.doi.org/10.1021/acs.orglett.0c00478
Org. Lett. 2020, 22, 2298–2302

Scheme 1. Halogenation of Ortho-Positions To Afford Fully Halogenated TAPPs

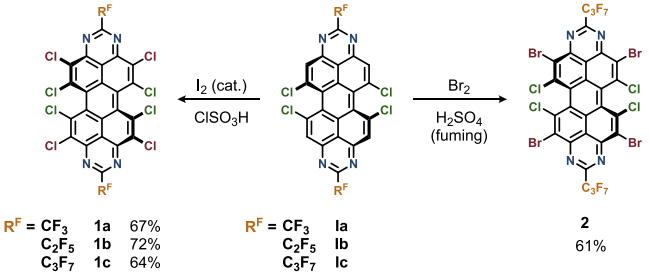

differently bay-substituted perylene and peropyrene systems (Figure 1).[12,45−47] However, the additional ortho-halogenation leads to an additional torsion of up to 12° between the vicinal substituents within the individual naphthalene subunits, a vicinal twist denoted as Φ. The opposing bay-substituents are thus pushed out of the plane in opposite directions, resulting in a reduced steric pressure in the bay-region and leading to a slight reduction of the molecule torsion angles δ.

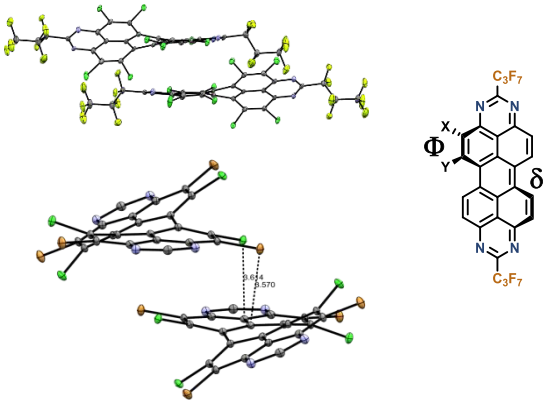

Figure 1. Solid-state structures of **1** (top) in side view and of **2** (bottom) in front view displaying intermolecular halogen−π distances (C_3F_7-groups are omitted for clarity). The core-twist angle δ and vicinal-twist Φ induced by the core substitution are indicated on the right.

A half-sided packing motif of adjacent molecules emerges due to the nonplanar molecular structure, whereas the remaining subunits of the TAPPs are twisted out of this plane (Figure 1). The intramolecular torsion induces a helical chirality in these systems that seems to play a significant role in the packing order, as they crystallize in a 1:1 ratio of P- and M-enantiomers with both stacking next to each other. A significant offset of adjacent molecules was observed for both **1** and **2** along with an elongation of π−π distances compared to **I** possibly representing reduced π−π interactions of neighboring molecules but orientation of the halogen substituents perpendicular to the π-plane of the next molecule. However, neither classical linear orientated halogen−π bonding nor direct halogen−halogen bonding was observed for these compounds. Analogous to the planar derivatives, the ortho-halogenation slightly increases the solubility of these compounds in CH_2Cl_2 from ca. 10 mg/mL to 21−26 mg/mL (**1a−c**) and 31 mg/mL (**2**), respectively.

The synthesis of the octahalogenated TAPPs allowed the investigation of the different effects of bay- and ortho-halogenation on the optical properties (Table 1).

Similar to the bay-chlorinated TAPP **I**, the fully functionalized TAPPs exhibit broadened absorption and emission bands (Figure 2) compared to the planar derivatives. Additionally, the ortho-halogenation results in a further bathochromic shift of the absorption maxima. The effect is similarly pronounced for **1** and **2**; however, the impact of the second halogenation step seems to be slightly diminished compared to the effect of the bay-halogenation. The ortho-halogenation influences the emission maxima in a similar fashion by a red shift of 46−56 nm (0.22−0.27 eV), along with slightly increased Stokes shifts for **1** and **2**.

The ortho-halogenation upon going from **I** to **1a−c** and **2** further impacts the redox potentials of the latter. As previously reported, tetrahalogenation at either the bay- or the ortho-positions of the TAPPs stabilizes the LUMO energies.[39−41] Hence, the fully core-halogenated TAPPs exhibit the lowest LUMO energies observed so far within the TAPP family (Table 2). They possess an equally pronounced electron deficiency as the similarly substituted PDI systems for which LUMO energies between −4.21 and −4.31 eV were derived.[22,34,49]

The redox potentials determined by cyclic voltammetry (Table 2, pp S17−S18 in Supporting Information (SI)), which are shifted to positive values (vs SCE) for the perhalogenated species, prompted us to chemically synthesize and isolate the corresponding reduced C_3F_7-substituted TAPP anions derived from **1c** and **2**. The stoichiometric addition of KC_8 as a one-electron reducing agent afforded the quantitative and selective formation of the mono- or dianionic species (Scheme 2).[15]

The monoanions $\mathbf{1c}^{\bullet-}$ and $\mathbf{2}^{\bullet-}$ were found to be remarkably stable toward degradation under ambient conditions and could be kept in solution for several hours, whereas the diamagnetic dianions, though thermally stable in solution under an inert gas atmosphere, immediately decomposed upon exposure to air. The marked difference in redox potential between $\mathbf{T}/\mathbf{T}^{\bullet-}$ and

Table 1. Structural and Photophysical Properties of Core-Halogenated TAPPs

	|Φ|[a] [deg]	|δ|[b] [deg]	π−π[c] [Å]	λ_{Abs}[d] [nm]	λ_{Em}[d] [nm]	Stokes shift [cm^{-1}]
TAPP-H	–	–	3.51	436	448	1454
I	–	32	3.60	474	484	936
1a	n/a	n/a	n/a	500	530	1132
1b	n/a	n/a	n/a	501	533	1198
1c	11.2 (0.3)	30.19 (0.06)	3.85	501	538	1372
2	12.8(0.2)	27.21 (0.04)	3.81	508	540	1166

[a]Vicinal-twist Φ was measured between adjacent halogen atoms and involved C atoms (error in parentheses). [b]Core-twist δ was measured between both diazaphenalenyl-planes of one molecule (error in parentheses). [c]π−π-distance was measured between two adjacent diazaphenalenyl-subunits. [d]Measured in THF.

https://dx.doi.org/10.1021/acs.orglett.0c00478
Org. Lett. 2020, 22, 2298−2302

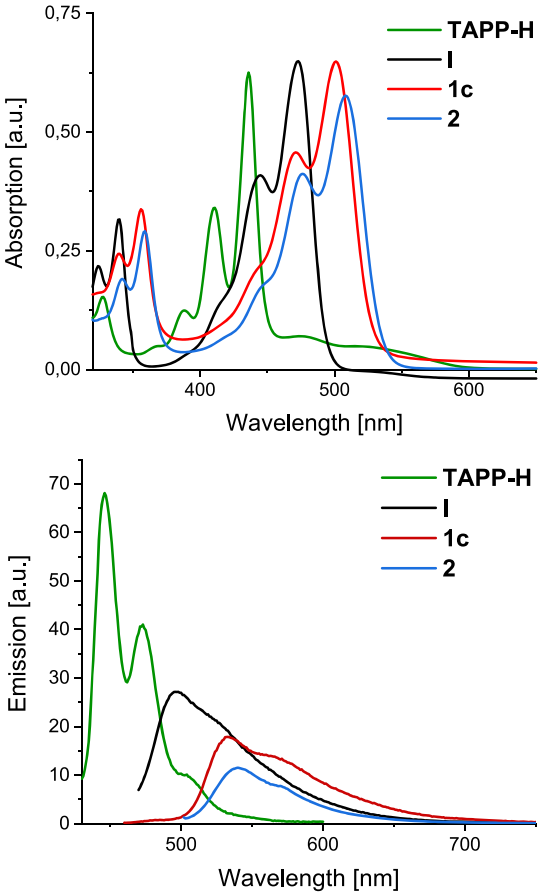

Figure 2. Absorption (top) and emission spectra (bottom) of fully halogenated TAPPs in THF (c = (1.2−1.6) × 10^{-5} M), compared to the bay-chlorinated (**I**) and unsubstituted (TAPP-H) TAPPs.

Table 2. Effect of the Bay- and Subsequent Ortho-Halogenation on the Electrochemical TAPP Properties

	E_{Red1} [V] [a]	E_{Red2} [V] [a]	E_{HOMO} [eV] [b]	E_{LUMO} [eV] [b,c]	EA [eV] [b]
TAPP-H	−0.53	−0.95	−6.61	−3.66	2.53
I	−0.19	−0.49	−6.91	−4.20	3.31
1a	0.15	−0.25	−6.75	−4.27	3.46
1b	0.16	−0.27	−6.77	−4.28	3.56
1c	0.16	−0.27	−6.78	−4.28	3.55
2	0.08	−0.30	−6.75	−4.30	3.50

[a]Measured against SCE in THF. [b]Calculated at B3LYP/def2-SVP level of theory. [c]Determination of LUMO levels according to literature methods by CV measurements using Fc/Fc+ as internal standard (E_{HOMO}(Fc) = −4.8 eV)[48] showed only insignificant deviation of up to 0.10 eV compared to the computed energies (see SI for further information).

$T^{\bullet-}/T^{2-}$ stabilized the radical monoanion toward disproportionation into the dianion and the neutral compound. The ESR spectra of both monoanionic species are characterized by featureless resonances with g-factors of 2.004 ($\mathbf{1c}^{\bullet-}$) and 2.005 ($\mathbf{2}^{\bullet-}$), which correspond to a completely delocalized organic radical (p S10 in SI) as expected if the NIR absorption band corresponds to a $\pi \rightarrow \pi^*$ transition (*vide infra*).

For both substitution patterns in **1c** and **2**, the first reduction step is accompanied by a drastic bathochromic shift of the $\pi \rightarrow \pi^*$ band from 501 to 702 nm and from 508 to 699 nm, respectively (Table SI, Figure 3) while further

Scheme 2. Reduction of 1 and 2 to Monoanionic and Dianionic TAPPs

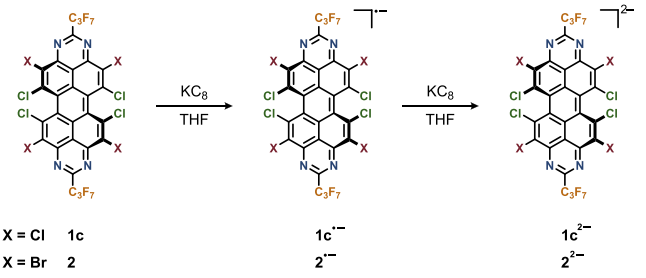

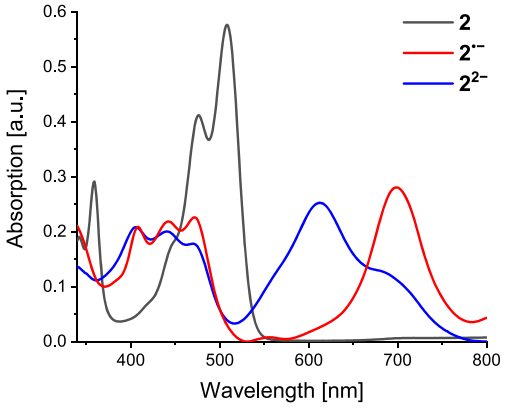

Figure 3. Absorption spectra of **2** and the corresponding monoanion $\mathbf{2}^{\bullet-}$ and dianion $\mathbf{2}^{2-}$ measured in THF (c = 1.2 × 10^{-5} M).

reduction to the dianion gave rise to a broadening of the bands and a significant blue shift to 607 and 613 nm (Table SI), respectively. None of the reduced species exhibit vibrational progression for the $\pi \rightarrow \pi^*$ band in contrast to the neutral compound.

In order to further analyze the photophysical properties of the reduced TAPPs, the vertical excitations of neutral, monoanionic, and dianionic species were computed using time-dependent density-functional theory (TDDFT) B3LYP/TZVPP employing the conductor-like screening model (COSMO) to ensure negative highest occupied molecular orbital (HOMO) energies for the anions (Table SI, Figure 4). The computed vertical transitions are in good agreement with the experimental data and reproduce the observed bathochromic (due to the first reduction) and subsequent hypsochromic shifts (due to the second reduction) accurately.

The absorption bands correspond to typical $\pi-\pi^*$-excitations, which may be viewed as $S_0 \rightarrow S_1$ excitations dominated by a HOMO → LUMO transition component for the closed-shell neutral and dianionic compounds. For the open-shell radical monoanions, the excitation corresponds to a $D_0 \rightarrow D_1$ transition, i.e. an excitation from the doublet ground state to the first excited doublet state, which is analyzed in terms of $HOMO_\alpha \rightarrow LUMO_\alpha$ and $HOMO_\beta \rightarrow LUMO_\beta$ contributions (Table SI).

While the vertical transitions computed using TDDFT are in good agreement with the experimental data (Table SI), this shows also that the one-particle picture, i.e. orbital-energy differences, has to be treated with care. While the TDDFT value of 533 nm (2.33 eV) is in qualitative agreement with the orbital-energy difference of 2.53 eV, the computed vertical transition of 661 nm (1.88 eV) corresponds to a shift of about 0.45 eV due to the first ionization, while the shift, when

https://dx.doi.org/10.1021/acs.orglett.0c00478
Org. Lett. 2020, 22, 2298−2302

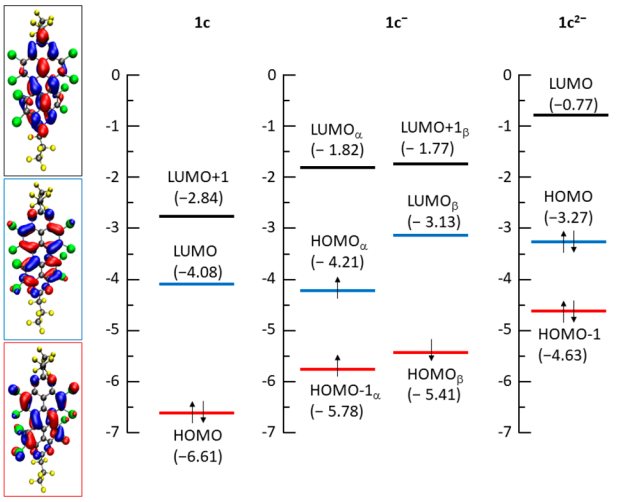

Figure 4. Molecular frontier orbitals of neutral, monoanionic, and dianionic compound **1c** and their orbital energies in eV, calculated at B3LYP/TZVPP level of theory employing COSMO.

estimated as the orbital-energy difference, only amounts to about 0.14 to 0.25 eV, corresponding to a relative error of about 45% to 70%.

As discussed above, the low-lying LUMO levels as well as the relatively high electron affinities render these materials potential n-channel semiconductors in organic electronic devices. Previous studies of TAPP derivatives revealed electron mobilities of up to 0.17 $cm^2/(V\ s)$,[41] whereas bay-functionalization perturbed the intermolecular packing order, resulting in smaller mobilities of about 10^{-3} $cm^2/(V\ s)$ for the bay-chlorinated derivative **I**.[45] The octachlorinated TAPP derivative **1c** was evaluated in bottom-gate, top-contact TFTs with a vacuum-deposited semiconductor layer (p S32 in SI). Although the molecular torsion in **1** does not differ significantly upon ortho-halogenation compared to the tetra-bay-chlorinated TAPP (**I**), the crystallinity of the film improved greatly, leading to an enhancement of the electron mobility by one order of magnitude to 0.014 $cm^2/(V\ s)$. The same observation was made by Bao et al. when comparing the tetra- and octachlorinated N-unsubstituted PDI.[35,50] The high electron mobility of the octachlorinated PDI (0.84 $cm^2/(V\ s)$) is likely due to the dense packing, which is induced by N−H···O hydrogen bonding, as an octabrominated PDI exhibits significantly reduced mobility (2×10^{-3} $cm^2/(V\ s)$).[32] Also, Bao and Würthner have found a significant dependency of the electron mobility on the planarity of the organic materials.[12] Unfortunately, the mixed halogenated TAPP **2** partially degraded upon sublimation, preventing the preparation of thin films by vacuum deposition.

In summary, a synthetic route was established that enables the access to fully core-halogenated TAPP systems. The octahalogenation not only stabilizes the reduced mono- and dianionic compounds sufficiently to allow for the preparation and characterization of these species but also led to an improvement of the electron mobility compared to the parent compound **I** when employed as an n-channel semiconductor in thin-film transistors. The core-perhalogenated TAPPs may play a role as key intermediates for subsequent derivatization, which will be the focus of future work in our laboratory.

■ ASSOCIATED CONTENT

Supporting Information

The Supporting Information is available free of charge at https://pubs.acs.org/doi/10.1021/acs.orglett.0c00478.

Experimental and computational details, data, and spectra (PDF)

Accession Codes

CCDC 1980430−1980431 contain the supplementary crystallographic data for this paper. These data can be obtained free of charge via www.ccdc.cam.ac.uk/data_request/cif, or by emailing data_request@ccdc.cam.ac.uk, or by contacting The Cambridge Crystallographic Data Centre, 12 Union Road, Cambridge CB2 1EZ, UK; fax: +44 1223 336033.

■ AUTHOR INFORMATION

Corresponding Author

Lutz H. Gade − *Anorganisch Chemisches Institut, Universität Heidelberg, 69120 Heidelberg, Germany;* orcid.org/0000-0002-7107-8169; Email: lutz.gade@uni-heidelberg.de

Authors

Benjamin A. R. Günther − *Anorganisch Chemisches Institut, Universität Heidelberg, 69120 Heidelberg, Germany*

Sebastian Höfener − *Karlsruher Institut für Technologie (KIT), 76131 Karlsruhe, Germany;* orcid.org/0000-0003-4504-347X

Robert Eichelmann − *Anorganisch Chemisches Institut, Universität Heidelberg, 69120 Heidelberg, Germany*

Ute Zschieschang − *Max Planck Institute for Solid State Research, 70569 Stuttgart, Germany*

Hubert Wadepohl − *Anorganisch Chemisches Institut, Universität Heidelberg, 69120 Heidelberg, Germany*

Hagen Klauk − *Max Planck Institute for Solid State Research, 70569 Stuttgart, Germany*

Complete contact information is available at: https://pubs.acs.org/10.1021/acs.orglett.0c00478

Notes

The authors declare no competing financial interest.

■ ACKNOWLEDGMENTS

This work has been supported by the Deutsche Forschungsgemeinschaft (DFG) within the collaborative research center SFB 1249 "N-Heteropolycycles as Functional Materials" (Projects A02, B07, and C01).

■ REFERENCES

(1) Shan, B.; Miao, Q. *Tetrahedron Lett.* **2017**, *58*, 1903−1911.
(2) Gao, X.; Hu, Y. *J. Mater. Chem. C* **2014**, *2*, 3099−3117.
(3) Nowak-Król, A.; Shoyama, K.; Stolte, M.; Würthner, F. *Chem. Commun.* **2018**, *54*, 13763−13772.
(4) Chen, L.; Li, C.; Müllen, K. *J. Mater. Chem. C* **2014**, *2*, 1938−1956.
(5) Zhang, G.; Zhao, J.; Chow, P. C. Y.; Jiang, K.; Zhang, J.; Zhu, Z.; Zhang, J.; Huang, F.; Yan, H. *Chem. Rev.* **2018**, *118*, 3447−3507.
(6) Yan, C.; Barlow, S.; Wang, Z.; Yan, H.; Jen, A. K.-Y.; Marder, S. R.; Zhan, X. *Nat. Rev. Mater.* **2018**, *3*, 18003−18020.
(7) De Leeuw, D. M.; Simenon, M. M. J.; Brown, A. R.; Einerhand, R. E. F. *Synth. Met.* **1997**, *87*, 53−59.
(8) Bunz, U. H. F. *Chem. - Eur. J.* **2009**, *15*, 6780−6789.

https://dx.doi.org/10.1021/acs.orglett.0c00478
Org. Lett. 2020, 22, 2298−2302

(9) Winkler, M.; Houk, K. N. *J. Am. Chem. Soc.* **2007**, *129*, 1805−1815.
(10) Tang, M. L.; Bao, Z. *Chem. Mater.* **2011**, *23*, 446−455.
(11) Zhan, X.; Facchetti, A.; Barlow, S.; Marks, T. J.; Ratner, M. A.; Wasielewski, M. R.; Marder, S. R. *Adv. Mater.* **2011**, *23*, 268−284.
(12) Schmidt, R.; Oh, J. H.; Sun, Y.-S.; Deppisch, M.; Krause, A.-M.; Radacki, K.; Braunschweig, H.; Könemann, M.; Erk, P.; Bao, Z.; et al. *J. Am. Chem. Soc.* **2009**, *131*, 6215−6228.
(13) Zaumseil, J.; Sirringhaus, H. *Chem. Rev.* **2007**, *107*, 1296−1323.
(14) Anthony, J. E.; Facchetti, A.; Heeney, M.; Marder, S. R.; Zhan, X. *Adv. Mater.* **2010**, *22*, 3876−3892.
(15) Ji, L.; Haehnel, M.; Krummenacher, I.; Biegger, P.; Geyer, F. L.; Tverskoy, O.; Schaffroth, M.; Han, J.; Dreuw, A.; Marder, T. B.; et al. *Angew. Chem., Int. Ed.* **2016**, *55*, 10498−10501.
(16) Ji, L.; Friedrich, A.; Krummenacher, I.; Eichhorn, A.; Braunschweig, H.; Moos, M.; Hahn, S.; Geyer, F. L.; Tverskoy, O.; Han, J.; et al. *J. Am. Chem. Soc.* **2017**, *139*, 15968−15976.
(17) Reiss, H.; Ji, L.; Han, J.; Koser, S.; Tverskoy, O.; Freudenberg, J.; Hinkel, F.; Moos, M.; Friedrich, A.; Krummenacher, I.; et al. *Angew. Chem., Int. Ed.* **2018**, *57*, 9543−9547.
(18) Kumar, Y.; Kumar, S.; Mandal, K.; Mukhopadhyay, P. *Angew. Chem., Int. Ed.* **2018**, *57*, 16318−16322.
(19) Kumar, S.; Malik, V.; Shukla, J.; Kumar, Y.; Bansal, D.; Chatterjee, R.; Mukhopadhyay, P. *Chem. - Eur. J.* **2019**, *25*, 4740−4750.
(20) Halasinski, T. M.; Weisman, J. L.; Ruiterkamp, R.; Lee, T. J.; Salama, F.; Head-Gordon, M. *J. Phys. Chem. A* **2003**, *107*, 3660−3669.
(21) Konkin, A.; Ritter, U.; Konkin, A. A.; Mamin, G.; Orlinskii, S.; Gafurov, M.; Aganov, A.; Klochkov, V.; Lohwasser, R.; Thelakkat, M.; et al. *J. Phys. Chem. C* **2018**, *122*, 22829−22837.
(22) Seifert, S.; Schmidt, D.; Würthner, F. *Chem. Sci.* **2015**, *6*, 1663−1667.
(23) Ghosh, I.; Ghosh, T.; Bardagi, J. I.; König, B. *Science (Washington, DC, U. S.)* **2014**, *346*, 725−728.
(24) Kumar, Y.; Kumar, S.; Bansal, D.; Mukhopadhyay, P. *Org. Lett.* **2019**, *21*, 2185−2188.
(25) Nowak-Król, A.; Würthner, F. *Org. Chem. Front.* **2019**, *6*, 1272−1318.
(26) Sun, M.; Müllen, K.; Yin, M. *Chemical Society Reviews*; Royal Society of Chemistry: March 14, 2016; pp 1513−1528.
(27) Soh, N.; Ueda, T. *Talanta*; Elsevier: September 15, 2011; pp 1233−1237.
(28) Huang, C.; Barlow, S.; Marder, S. R. *J. Org. Chem.* **2011**, *76*, 2386−2407.
(29) Würthner, F.; Stolte, M. *Chem. Commun.* **2011**, *47*, 5109−5115.
(30) Tang, M. L.; Oh, J. H.; Reichardt, A. D.; Bao, Z. *J. Am. Chem. Soc.* **2009**, *131*, 3733−3740.
(31) Jozeliunaite, A.; Striela, R.; Labanauskas, L.; Orentas, E. *Synthesis* **2017**, *49*, 5176−5182.
(32) Kumar, Y.; Kumar, S.; Kumar Keshri, S.; Shukla, J.; Singh, S. S.; Thakur, T. S.; Denti, M.; Facchetti, A.; Mukhopadhyay, P. *Org. Lett.* **2016**, *18*, 472−475.
(33) Gao, J.; Xiao, C.; Jiang, W.; Wang, Z. *Org. Lett.* **2014**, *16*, 394−397.
(34) Yue, W.; Jiang, W.; Böckmann, M.; Doltsinis, N. L.; Wang, Z. *Chem. - Eur. J.* **2014**, *20*, 5209−5213.
(35) Gsänger, M.; Oh, J. H.; Könemann, M.; Höffken, H. W.; Krause, A. M.; Bao, Z.; Würthner, F. *Angew. Chem., Int. Ed.* **2010**, *49*, 740−743.
(36) Riehm, T.; De Paoli, G.; Konradsson, A. E.; De Cola, L.; Wadepohl, H.; Gade, L. H. *Chem. - Eur. J.* **2007**, *13*, 7317−7329.
(37) Hahn, L.; Öz, S.; Wadepohl, H.; Gade, L. H. *Chem. Commun.* **2014**, *50*, 4941−4943.
(38) Hahn, L.; Buurma, N. J.; Gade, L. H. *Chem. - Eur. J.* **2016**, *22*, 6314−6322.
(39) Martens, S. C.; Zschieschang, U.; Wadepohl, H.; Klauk, H.; Gade, L. H. *Chem. - Eur. J.* **2012**, *18*, 3498−3509.
(40) Geib, S.; Zschieschang, U.; Gsänger, M.; Stolte, M.; Würthner, F.; Wadepohl, H.; Klauk, H.; Gade, L. H. *Adv. Funct. Mater.* **2013**, *23*, 3866−3874.
(41) Hahn, L.; Maaß, F.; Bleith, T.; Zschieschang, U.; Wadepohl, H.; Klauk, H.; Tegeder, P.; Gade, L. H. *Chem. - Eur. J.* **2015**, *21*, 17691−17700.
(42) Hahn, L.; Hermannsdorfer, A.; Günther, B.; Wesp, T.; Bühler, B.; Zschieschang, U.; Wadepohl, H.; Klauk, H.; Gade, L. H. *J. Org. Chem.* **2017**, *82*, 12492−12502.
(43) Martens, S. C.; Riehm, T.; Geib, S.; Wadepohl, H.; Gade, L. H. *J. Org. Chem.* **2011**, *76*, 609−617.
(44) Geib, S.; Martens, S. C.; Märken, M.; Rybina, A.; Wadepohl, H.; Gade, L. H. *Chem. - Eur. J.* **2013**, *19*, 13811−13822.
(45) Günther, B. A. R.; Höfener, S.; Zschieschang, U.; Wadepohl, H.; Klauk, H.; Gade, L. H. *Chem. - Eur. J.* **2019**, *25*, 14669−14678.
(46) Würthner, F. *Pure Appl. Chem.* **2006**, *78*, 2341−2349.
(47) Delgado, M. C. R.; Kim, E. G.; Da Silva Filho, D. A.; Bredas, J. L. *J. Am. Chem. Soc.* **2010**, *132*, 3375−3387.
(48) Seguy, I.; Jolinat, P.; Destruel, P.; Mamy, R.; Allouchi, H.; Courseille, C.; Cotrait, M.; Bock, H. *ChemPhysChem* **2001**, *2*, 448−452.
(49) Kumar, S.; Shukla, J.; Kumar, Y.; Mukhopadhyay, P. *Org. Chem. Front.* **2018**, *5*, 2254−2276.
(50) Ling, M. M.; Erk, P.; Gomez, M.; Koenemann, M.; Locklin, J.; Bao, Z. *Adv. Mater.* **2007**, *19*, 1123−1127.

https://dx.doi.org/10.1021/acs.orglett.0c00478
Org. Lett. 2020, 22, 2298−2302

Supporting Information

Perhalogenated Tetraazaperopyrenes and their corresponding Mono- and Dianions

Benjamin A. R. Günther,[a] Sebastian Höfener,[b] Robert Eichelmann,[a] Ute Zschieschang,[c] Hubert Wadepohl,[a] Hagen Klauk,[c] Lutz H. Gade*[a]

[a]Anorganisch-Chemisches Institut, Universität Heidelberg, Im Neuenheimer Feld 270, 69120 Heidelberg, Germany, Fax: (+49)6221545609

[b]Institute of Physical Chemistry, Karlsruhe Institute of Technology, (KIT) P.O. Box 6980, D-76049 Karlsruhe, Germany

[c]Max Planck Institute for Solid State Research, Heisenbergstr.1, 70569 Stuttgart, Germany

E-Mail: lutz.gade@uni-heidelberg.de

Table of Contents

General Information

General Procedures:

2,9-Bistrifluoroacetyl-5,6,12,13-tetrachloro-1,3,8,10-tetraazaperopyren (**Ic**), 2,9-Bisperfluoropropionyl-5,6,12,13-tetrachloro-1,3,8,10-tetraazaperopyren (**Ib**) and 2,9-Bisperfluorobutyryl-5,6,12,13-tetrachloro-1,3,8,10-tetraazaperopyren (**Ic**) were synthesized according to previously reported procedures.[S1]

All reagents were obtained from commercial sources and used as received without additional purification. Deuterated solvents were purchased from Deutero GmbH and used without further purification.

NMR-Spectroscopy:

^{13}C and ^{19}F NMR spectra were recorded with either a Bruker Avance III 600 or Bruker Avance II 400 spectrometer and quoted in ppm using the residual solvent peak as internal standard for ^{13}C NMR spectroscopy. $CFCl_3$ was used as reference in ^{19}F NMR spectra. The following abbreviations were used: s = singulet, d = dublet, t = triplet, q = quartet. Carbon atoms of TAPP derivatives were assigned as follows:

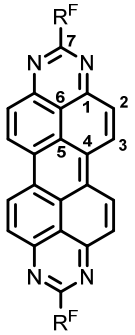

Mass Spectrometry:

Mass spectra were recorded by the Institute of Organic Chemistry of the Universität Heidelberg on a JMS 700 magnetic sector (Jeol) in FAB (NBA or NPOE as matrix) and ESI spectra on a Finnigan TSQ-7000, Finnigan LCQ quadrupole ion trap or a Burker apex-Qe hybrid 9.4 T FT-ICR (for HR-ESI) spectrometer.

UV/Vis and Fluorescence Spectroscopy:

The solvents used for spectroscopic studies were of spectroscopic grade and used as received. UV/Vis absorption spectra were recorded with a Cary 5000 UV/Vis/NIR spectrophotometer and were baseline- and solvent-corrected. Emission spectra were measured with a Varian Cary Eclipse spectrophotometer and standard corrections were applied to all spectra.

Cyclic Voltammetry:

Cyclic voltammetry was performed with a standard commercial electrochemical analyser in a three electrode single-component cell under argon. A platinum disk was used as the working electrode, a platinum wire as the counter electrode and a saturated calomel electrode as the reference electrode. All potentials were internally referenced to ferrocene. Dry THF was used as solvent and as supporting electrolyte tetrabutylammonium hexafluorophosphate was used. The measurements were carried out under exclusion of air and moisture.

Synthesis and Characterization of Compounds

Compound **1a**

150 mg of **Ia** (248.30 mmol, 1 eq.) and 43 mg of I_2 (169.42 mmol, 0.68 eq.) were dissolved in 5 ml of $ClSO_3H$. The reaction mixture was stirred at 120 °C in an oil bath for five days. After cooling to r.t., the reaction mixture was slowly given onto ice (Caution: $ClSO_3H$ reacts violently with H_2O to form HCl and H_2SO_4!), the resulting precipitate was filtered and washed with H_2O, methanol and pentane to yield the product as an orange powder (124 mg, 167.14 mmol, 67%).

^{13}C-NMR ($CDCl_3$, 150.90 MHz, 295 K): δ [ppm] = 152.0 (C-1), 139.0 (C-3), 135.7 (C-2), 126.0 (C-4), 122.3 (C-5), 113.4 (C-6).

^{19}F-NMR ($CDCl_3$, 376.27 MHz, 295 K): δ [ppm] = −68.7 (s, 6 F, CF_3).

HRMS (MALDI$^-$): calc. for $C_{28}{}^{35}Cl_6{}^{37}Cl_2F_{14}N_4$ [M^-]: 741.7476, found: 741.7484.

UV/Vis (THF): λ_{max} (log ε) = 500 (4.75).

Melting Point: Decomposition above 220°C.

LUMO energy determined by Cyclovoltammetry: E = −4.36 eV.

Compound **1b**

100 mg of **Ib** (142.02mmol, 1 eq.) and 15 mg of I_2 (59.1 mmol, 0.42 eq.) were dissolved in 5 ml of $ClSO_3H$. The reaction mixture was stirred at 120 °C in an oil bath for five days. After cooling to r.t., the reaction mixture was slowly given onto ice (Caution: $ClSO_3H$ reacts violently with H_2O to form HCl and H_2SO_4!), the resulting precipitate was filtered and washed with H_2O, methanol and pentane to yield the product as an orange powder (86 mg, 102.15 mmol, 72%).

^{13}C-NMR ($CDCl_3$, 150.90 MHz, 295 K): δ [ppm] = 156.4 (t, $^2J_{C\text{-}F}$ = 26.0 Hz, C-7), 152 (C-1), 139.0 (C-3), 135.8 (C-2), 126.1 (C-4), 122.3 (C-5), 113.3 (C-6).

^{19}F-NMR ($CDCl_3$, 376.27 MHz, 295 K): δ [ppm] = −81.5 (t, 6 F, $^3J_{F\text{-}F}$ = 1.7 Hz, CF_3), −115.3 (d, $^3J_{F\text{-}F}$ = 65.0 Hz, 4 F, CF_2).

HRMS (MALDI$^-$): calc. for $C_{26}{}^{35}Cl_6{}^{37}Cl_2F_{10}N_4$ [M^-]: 841.7412, found: 841.7417.

UV/Vis (THF): λ_{max} (log ε) = 501 (4.19).

Melting Point: Decomposition above 220°C.

LUMO energy determined by Cyclovoltammetry: E = −4.39 eV.

Compound **1c**

100 mg of **Ic** (124.36 mmol, 1 eq.) and 15 mg of I_2 (59.1 mmol, 0.48 eq.) were dissolved in 5 ml of $ClSO_3H$. The reaction mixture was stirred at 120 °C in an oil bath for five days. After cooling to r.t., the reaction mixture was cautiously given onto ice, the resulting precipitate was filtered and washed with H_2O, methanol and pentane to yield the product as an orange powder (75 mg, 79.63 mmol, 64%).

^{13}C-NMR ($CDCl_3$, 150.90 MHz, 295 K): δ [ppm] = 152.0 (C-1), 139.0 (C-3), 135.8 (C-2), 126.1 (C-4), 122.3 (C-5), 113.3 (C-6).

^{19}F-NMR ($CDCl_3$, 376.27 MHz, 295 K): δ [ppm] = −79.9 (t, 6 F, $^3J_{F\text{-}F}$ = 8.9 Hz, CF_3), −112.6-−114.5 (m, 4 F, CF_2), −125.2 (bs, 4 F, CF_2).

HRMS (MALDI$^-$): calc. for $C_{28}{}^{35}Cl_6{}^{37}Cl_2F_{14}N_4$ [M^-]: 941.7351, found: 941.7354.

UV/Vis (THF): λ_{max} (log ε) = 501 (4.35).

Melting Point: Decomposition above 220°C.

LUMO energy determined by Cyclovoltammetry: E = −4.39 eV.

Compound **2**

To a solution of 638 mg of **I** (0.79 mmol, 1 eq.) and 50.3 mg of I_2 (0.20 mmol, 0.25 eq.) in 20 ml fuming sulfuric acid (20% SO_3), 1.46 ml of bromine (28.5 mmol, 36 eq.) were added. The reaction was stirred at 120 °C for seven days. After cooling to r.t., the reaction was slowly poured on a mixture of ice and an aqueous $Na_2S_2O_5$ solution. Purification via column chromatography (SiO_2, petroleum ether/ethyl acetate 10:1) afforded the pure product as an orange solid (538 mg, 389 mmol, 61%).

^{13}C-NMR ($CDCl_3$, 150.90 MHz, 295 K): δ [ppm] = 153.0 (C-1), 141.5 (C-3), 128.9 (C-2), 126.1 (C-4), 122.7 (C-5), 112.7 (C-6).

^{19}F-NMR ($CDCl_3$, 376.27 MHz, 295 K): δ [ppm] = −79.9 (t, 6 F, $^3J_{F\text{-}F}$ = 8.9 Hz, CF_3), −112.6-−114.5 (m, 4 F, CF_2), −125.2 (bs, 4 F, CF_2).

HRMS (MALDI$^-$): calc. for $C_{28}{}^{79}Br_2{}^{81}Br_2{}^{35}Cl_3{}^{37}Cl_1F_{14}N_4$ [M^-]: 1119.5317, found: 1119.5313.

UV/Vis (THF): λ_{max} (log ε) = 508 (4.68).

Melting Point: Decomposition above 220°C.

LUMO energy determined by Cyclovoltammetry: E = −4.33 eV.

Synthesis of Reduced Compounds of 1c and 2

Compound **1c^{-}**

In a glove-box, 10 mg of **1c** (10.6 μmol, 1 eq.) were dissolved in 2 ml THF and treated with an equimolar amount of KC_8 (1.4 mg, 10.6 μmol, 1 eq.). The reaction mixture was stirred at r.t. for 10 min. The precipitate was filtered off and the solvent was removed *in vacuo* to yield the product as a green solid (9.4 mg, 9.6 μmol, 90%).

EPR (DCM, 9.63 GHz, 295 K): g = 2.004.

UV/Vis (THF): λ_{max} = 702.

Compound **2^{-}**

In a glove-box, 14 mg of **2** (12.5 μmol, 1 eq.) were dissolved in 2 ml THF and treated with 1.7 mg of KC_8 (12.5 μmol, 1 eq.). The reaction mixture was filtered after stirring for 10 min at r.t., and the solvent was removed *in vacuo*. The product was isolated as a green solid (13.8 mg, 11.9 μmol, 95%).

EPR (DCM, 9.63 GHz, 295 K): g = 2.005.

UV/Vis (THF): λ_{max} = 699.

Compound **1c^{2-}**

In a glovebox, 15 mg of neutral compound **1c** (15.9 μmol, 1 eq) were d issolved in 5 ml THF and treated with 4.5 mg of KC_8 (33.4 μmol, 2.1 eq), whereupon immediate color change of the solution to purple was observed. After filtration of the reaction mixture, the solvent was removed *in vacuo* to yield the desired product as purple powder (14.7 mg, 14.4 μmol, 90%).

UV/Vis (THF): λ_{max} = 607.

Compound **2^{2-}**

In a glovebox, 17 mg of neutral compound **2** (15.2 μmol, 1 eq) were dissolved in 5 ml THF and treated with 4.3 mg of KC_8 (31.9 μmol, 2.1 eq), whereupon immediate color change of the solution to purple was observed. After filtration of the reaction mixture, the solvent was removed in vacuo to yield the desired product as purple powder (17.5 mg, 14.6 μmol, 96%).

UV/Vis (THF): λ_{max} = 613.

The ^{1}H, ^{13}C and ^{19}F NMR Spectra of Compounds

Compound **1a**

^{13}C-NMR (150.90 MHz, $CDCl_3$, 295 K):

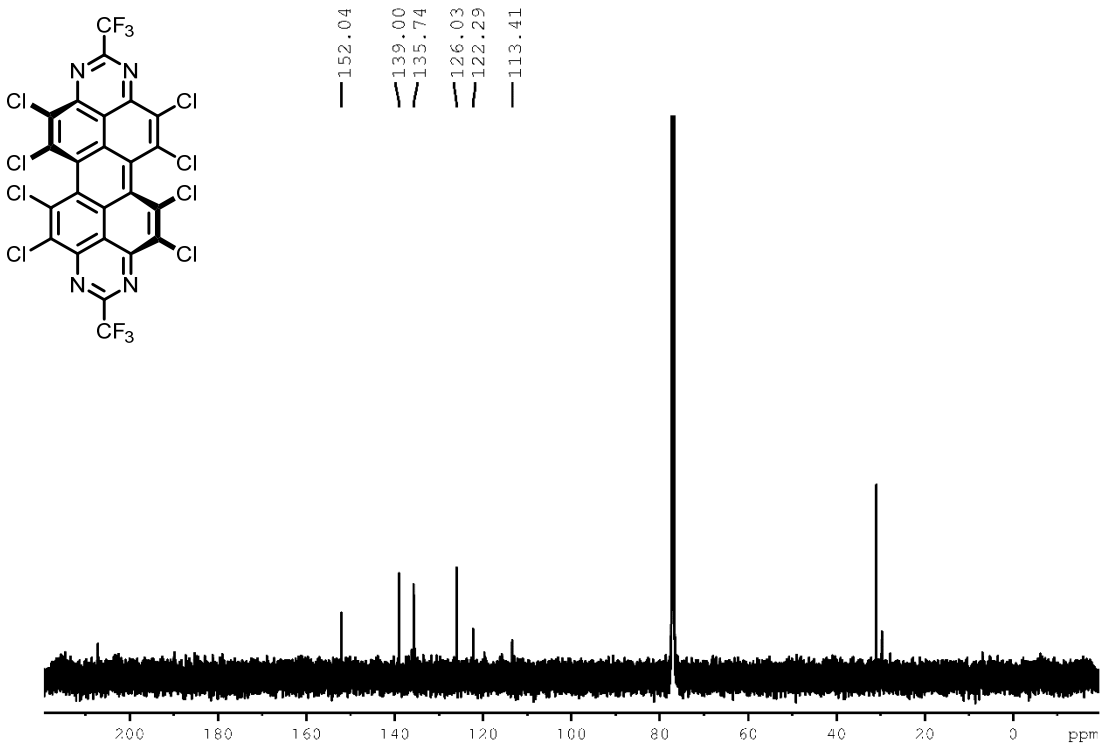

^{19}F-NMR (376.27 MHz, $CDCl_3$, 295 K):

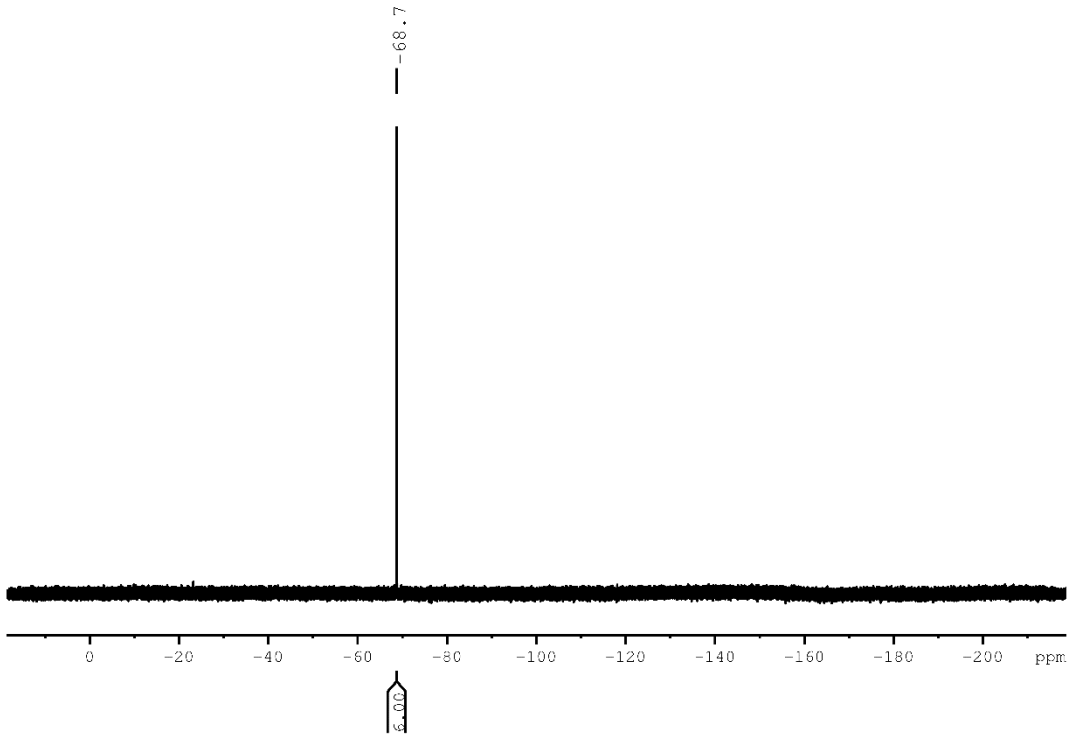

Compound **1b**

^{13}C-NMR (150.90 MHz, $CDCl_3$, 295 K):

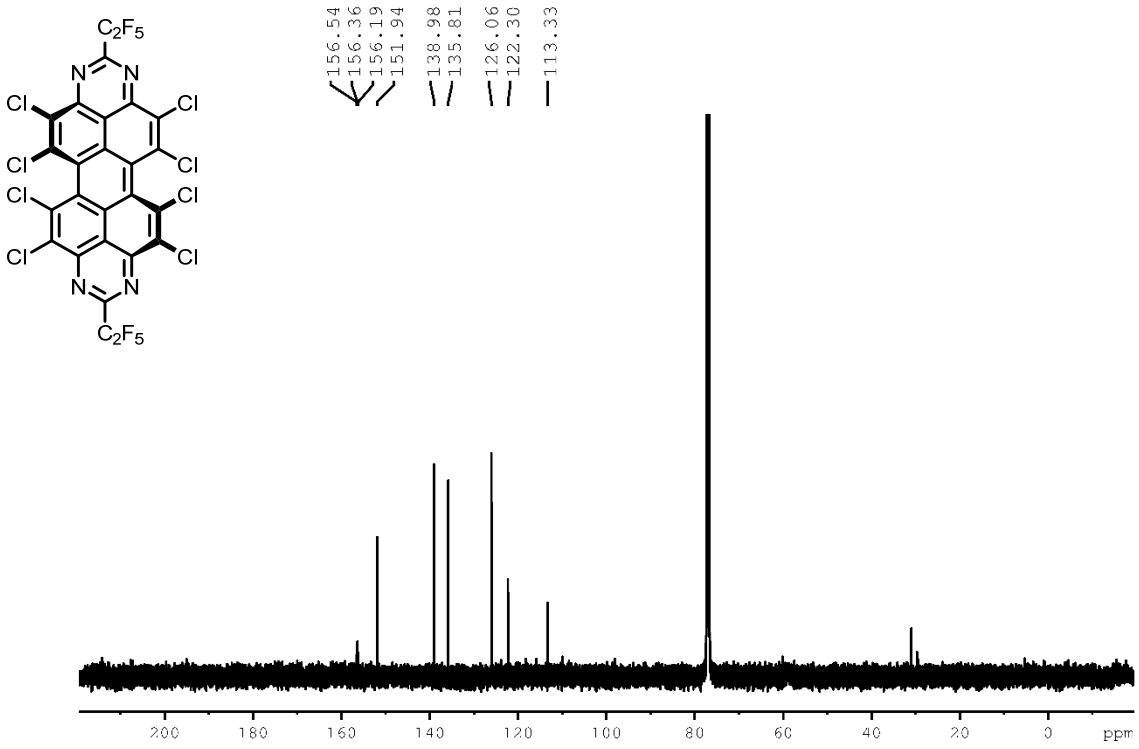

^{19}F-NMR (376.27 MHz, $CDCl_3$, 295 K):

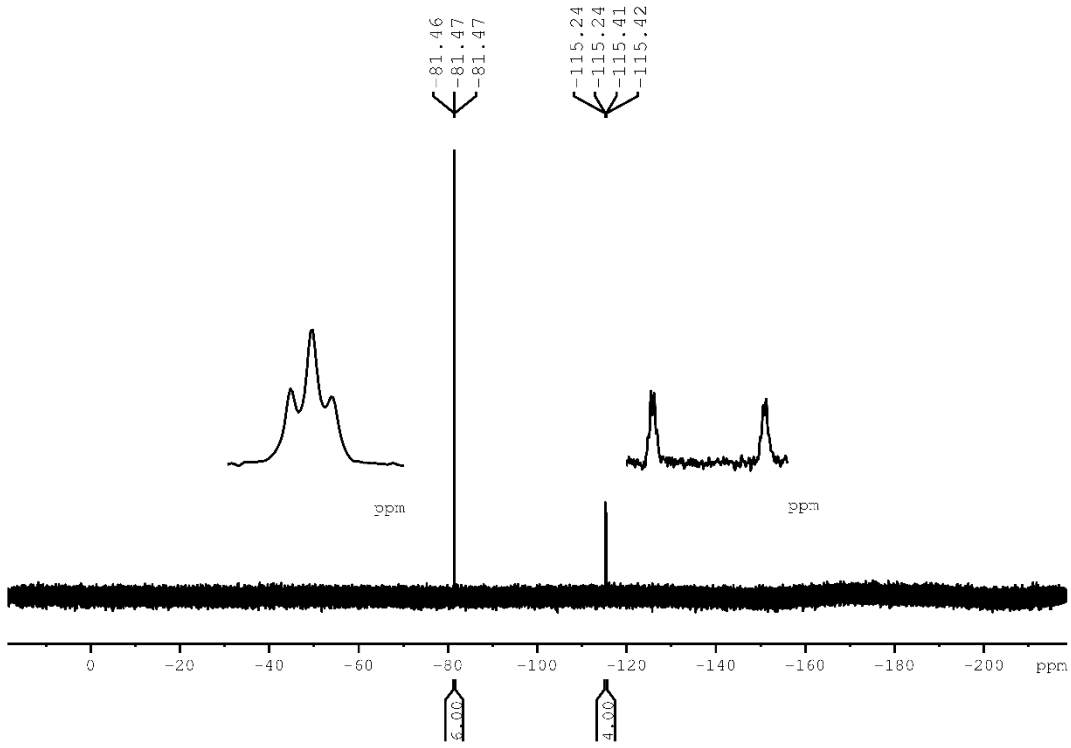

Compound **1c**

^{13}C-NMR (150.90 MHz, $CDCl_3$, 295 K):

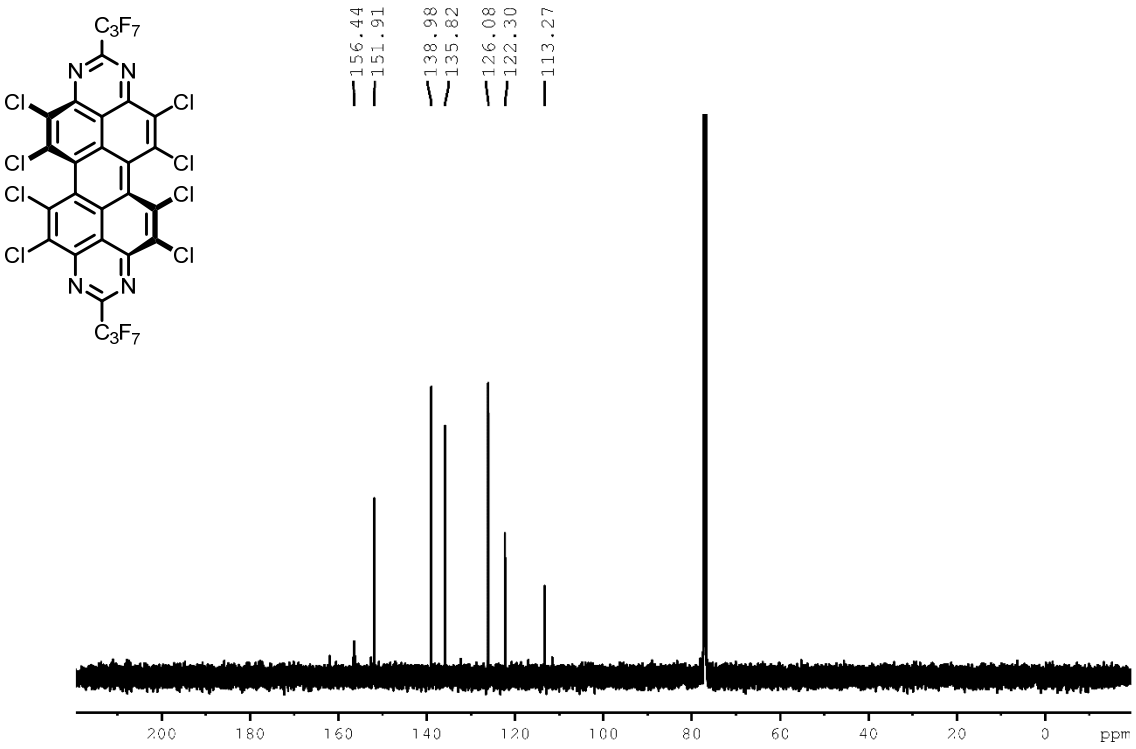

^{19}F-NMR (376.27 MHz, $CDCl_3$, 295 K):

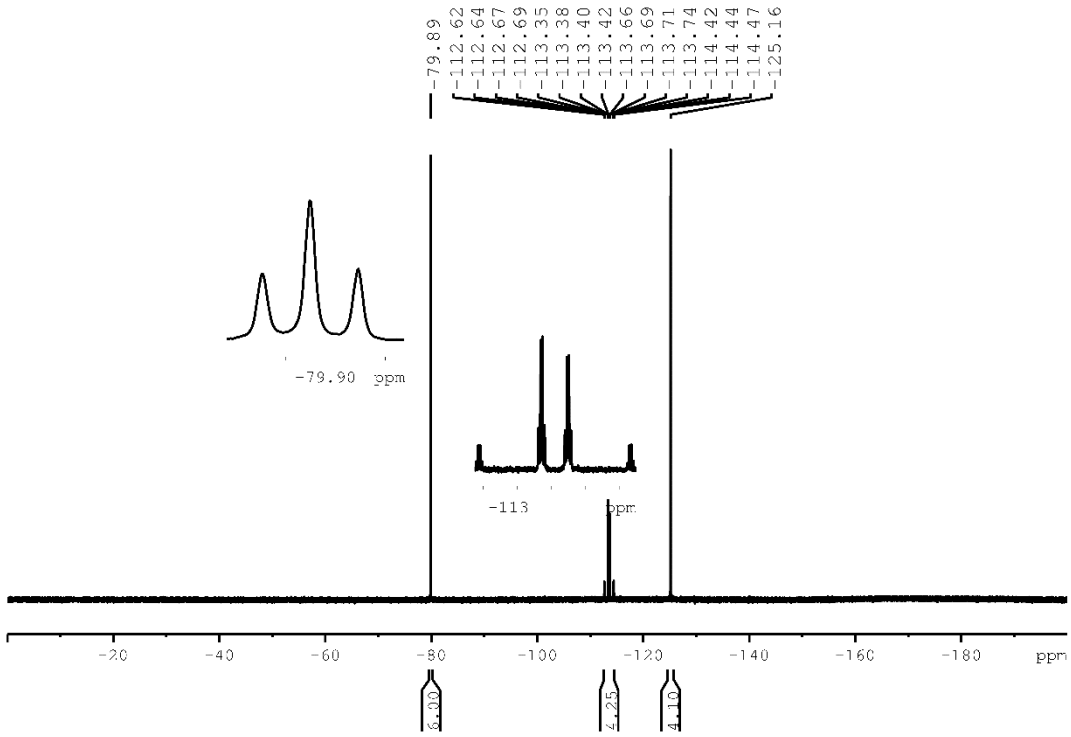

Compound **2**

^{13}C-NMR (150.90 MHz, $CDCl_3$, 295 K):

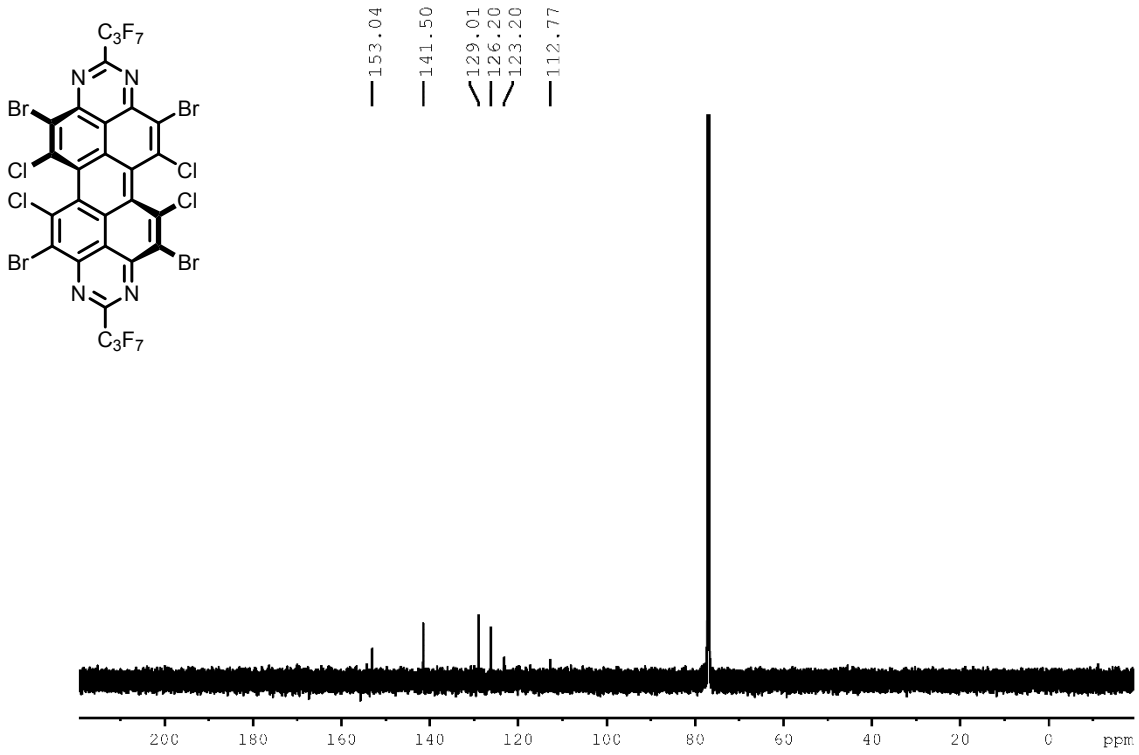

^{19}F-NMR (376.27 MHz, $CDCl_3$, 295 K):

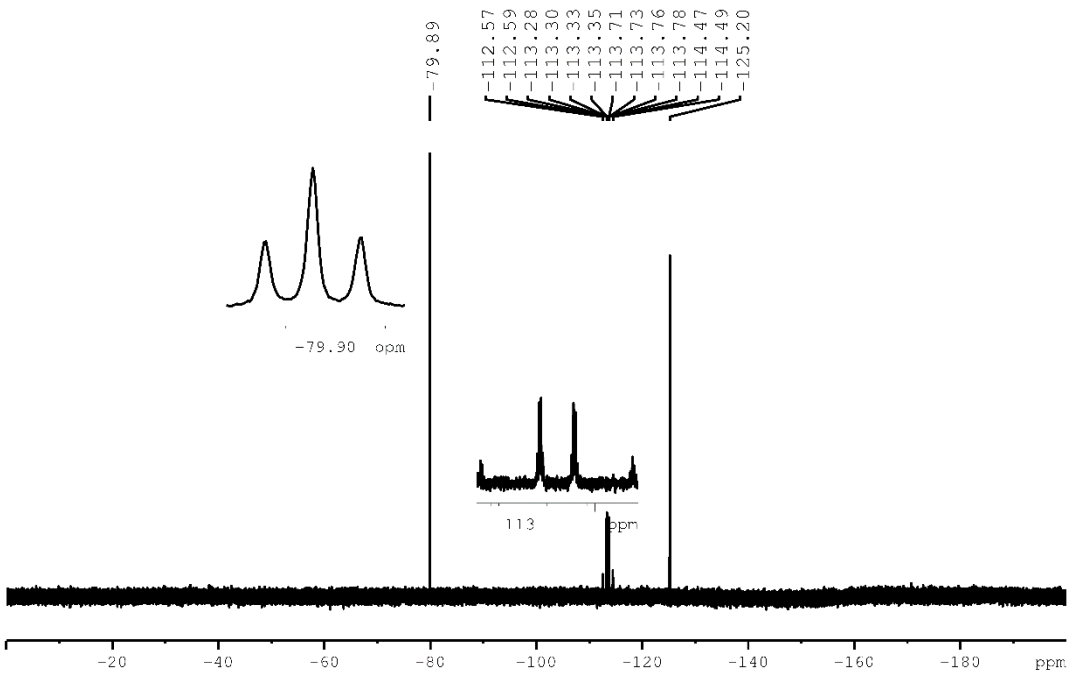

EPR Spectra of Monoanionic Compounds

Compound **1c**$^{\bullet-}$

EPR (dcm, 9.63 GHz, 295 K, c = 2.2×10^{-3} M):

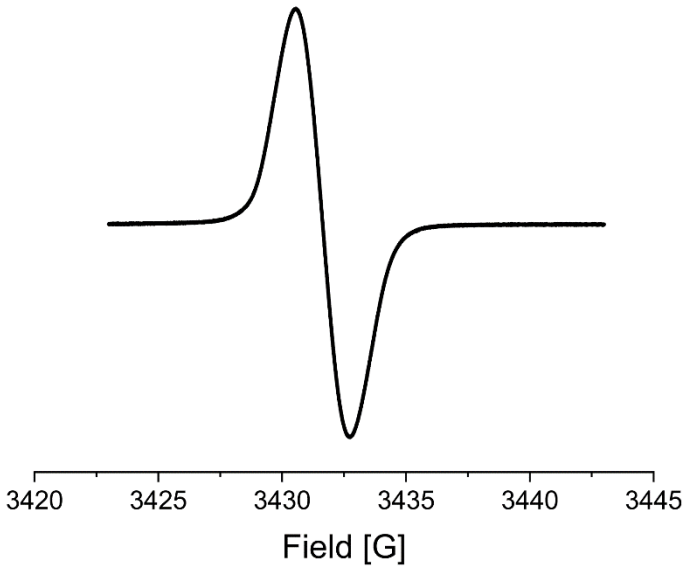

Compound **2**$^{\bullet-}$

EPR (dcm, 9.63 GHz, 295 K, c = 3.1×10^{-3} M):

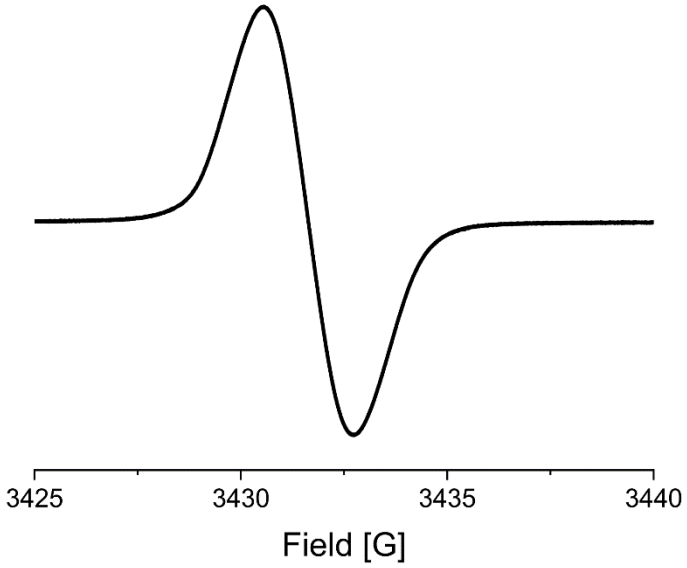

Absorption Spectra of Compounds

Compound **1a**

UV/vis (thf, 295 K, c = 6.1×10^{-5} M):

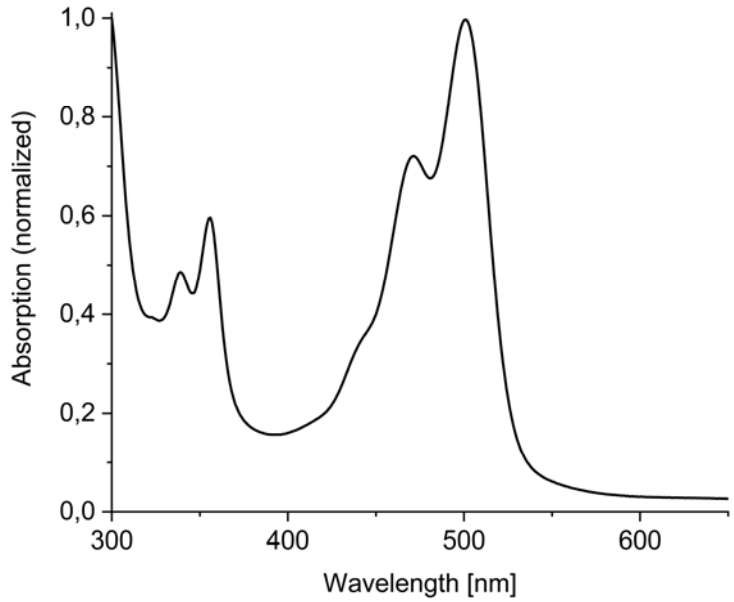

Compound **1b**

UV/vis (thf, 295 K, c = 3.2×10^{-5} M):

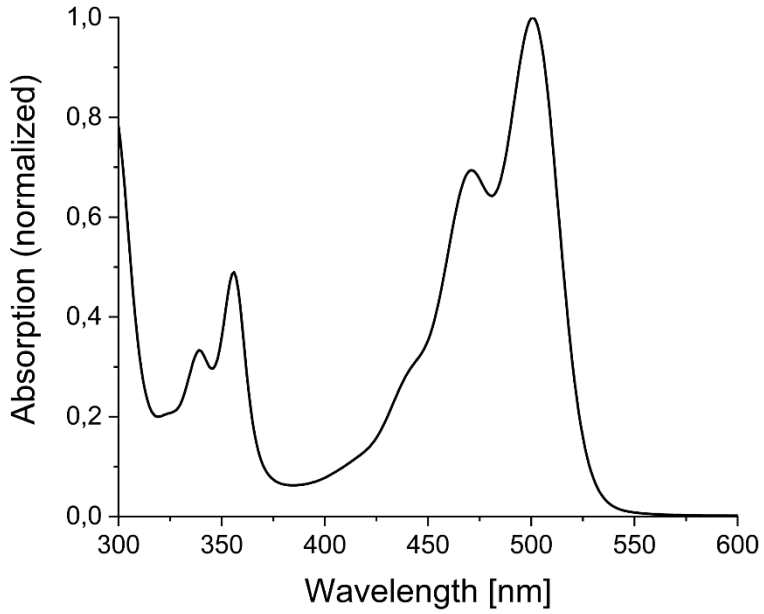

Compound **1c**

UV/vis (thf, 295 K, c = 1.6×10^{-5} M):

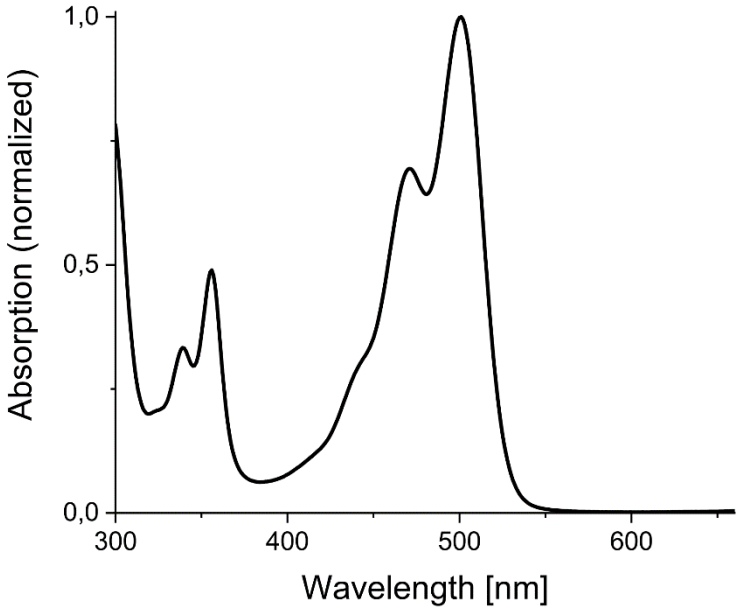

Compound **1c**$^{\bullet-}$

UV/vis (thf, 295 K, c = 1.6×10^{-5} M):

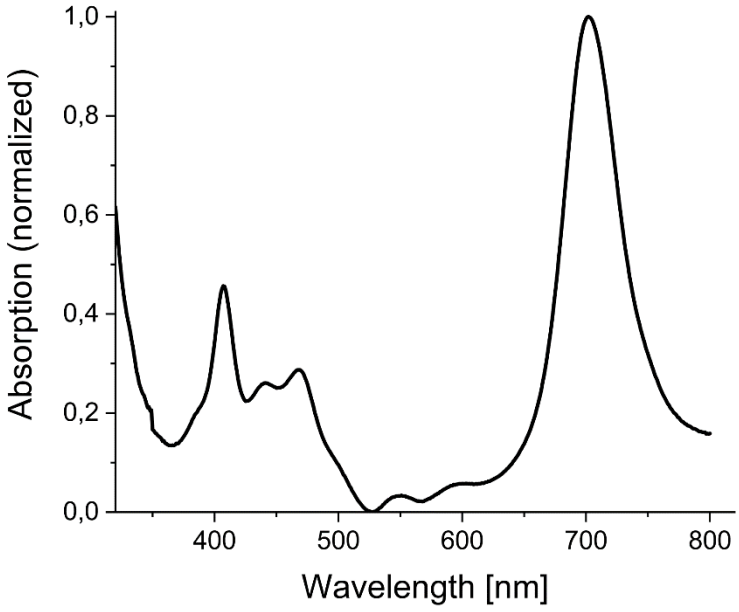

Compound **1c**$^{2-}$

UV/vis (thf, 295 K, c = 1.6×10^{-5} M):

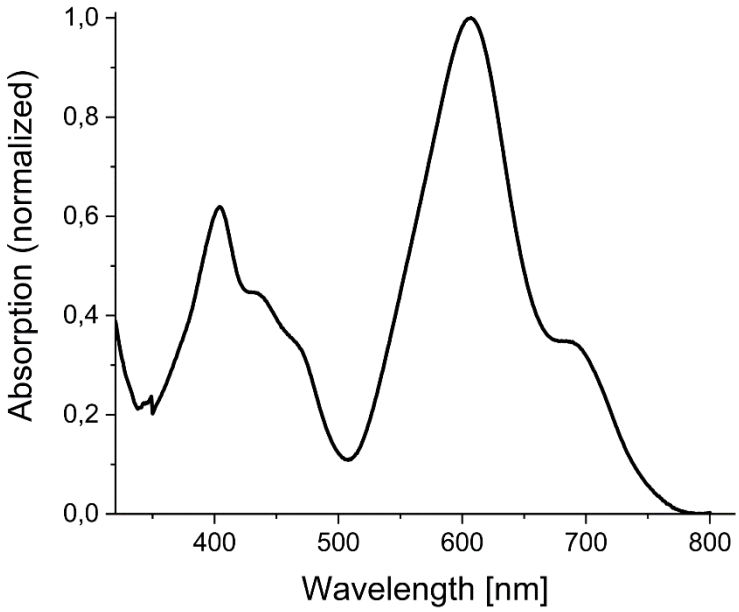

Compound **2**

UV/vis (thf, 295 K, c = 1.2×10^{-5} M):

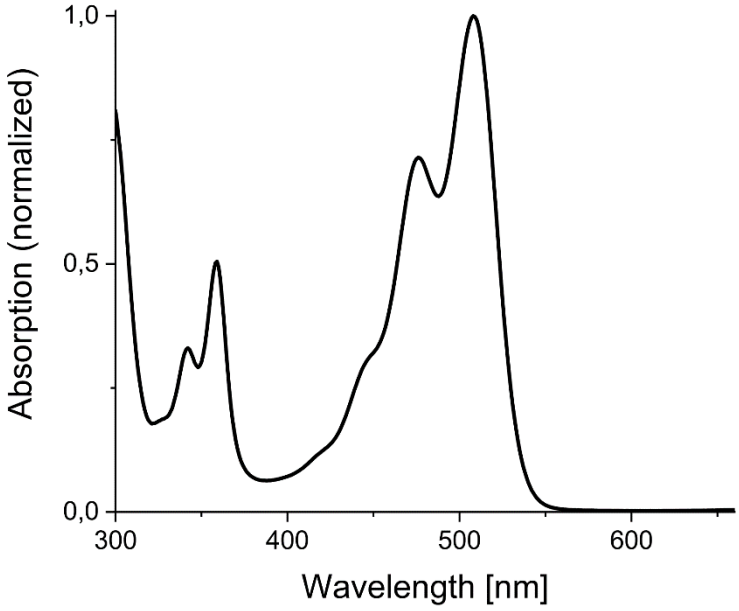

Compound $\mathbf{2}^{\bullet-}$

UV/vis (thf, 295 K, c = 1.2×10^{-5} M):

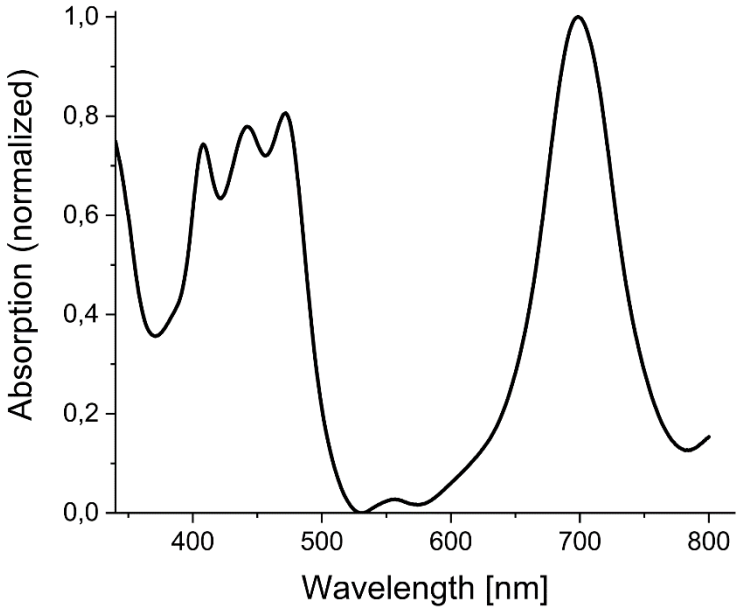

Compound $\mathbf{2}^{2-}$

UV/vis (thf, 295 K, c = 1.2×10^{-5} M):

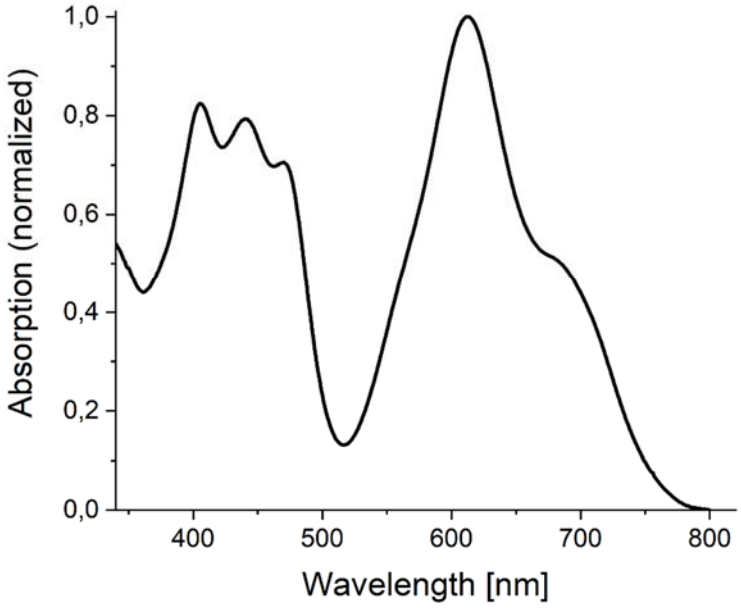

Emission Spectra of Compounds

Compound **1a**

Emission (thf, 295 K, c = 6.1×10^{-5} M):

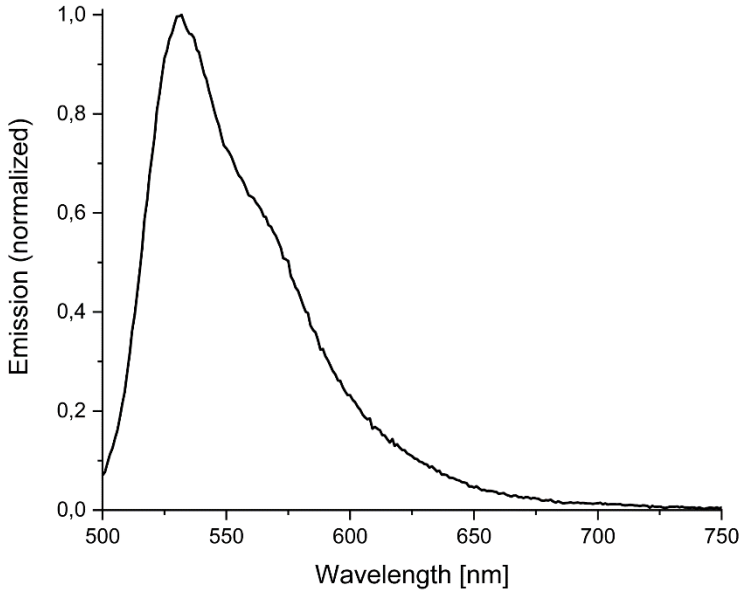

Compound **1b**

Emission (thf, 295 K, c = 3.2×10^{-5} M):

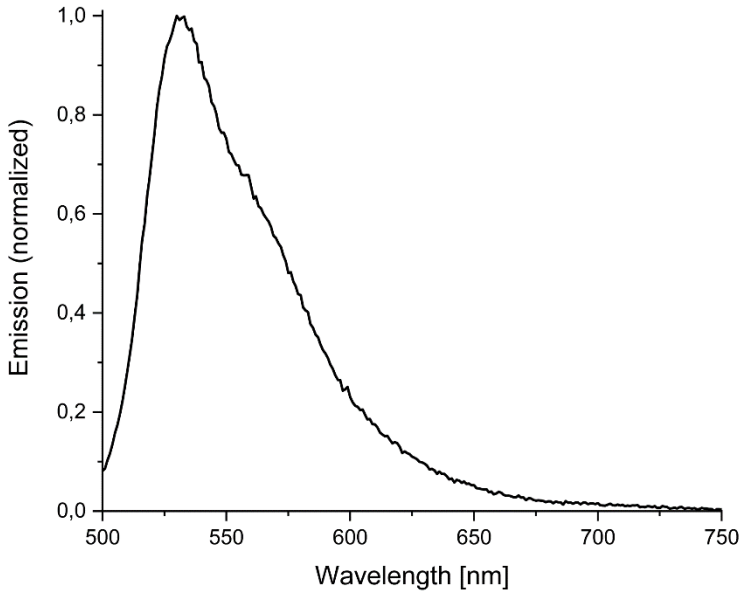

Compound **1c**

Emission (thf, 295 K, c = 1.6×10^{-5} M):

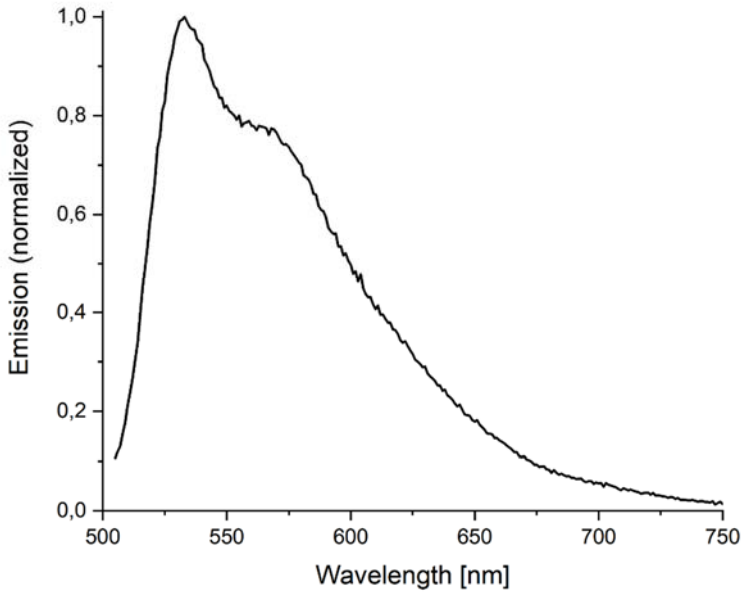

Compound **2**

Emission (thf, 295 K, c = 1.2×10^{-5} M):

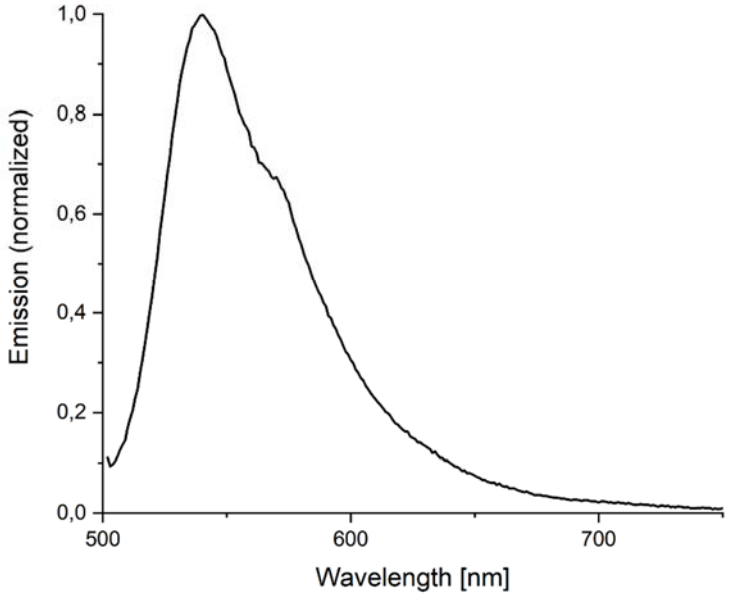

Cyclic Voltammograms of Compounds

Compound **1a**

(in dcm, sweep rate 50 mV/s; supporting electrolyte: NBu_4PF_6 (0.1 M); reference SCE)

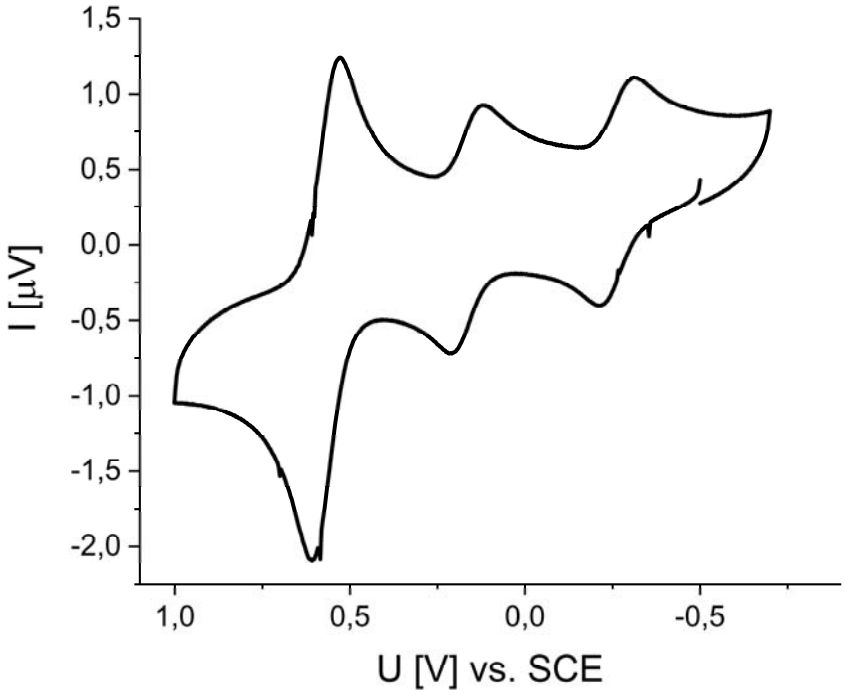

Compound **1b**

(in dcm, sweep rate 50 mV/s; supporting electrolyte: NBu_4PF_6 (0.1 M); reference SCE)

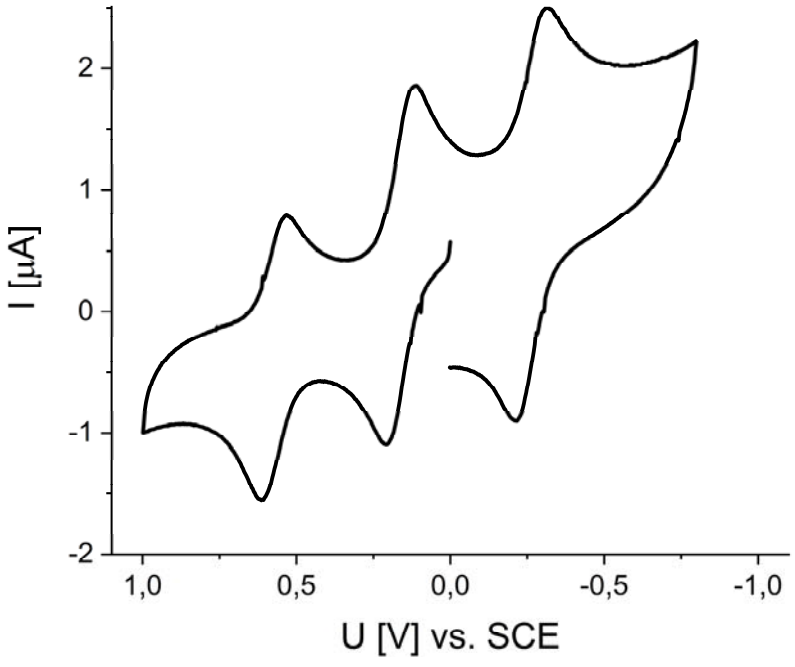

Compound **1c**

(in dcm, sweep rate 50 mV/s; supporting electrolyte: NBu_4PF_6 (0.1 M); reference SCE)

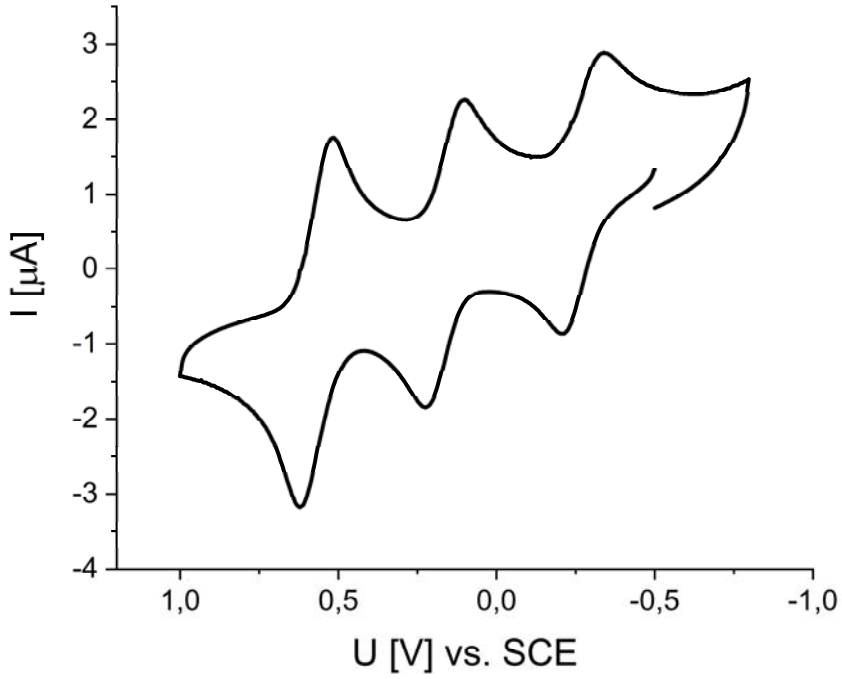

Compound **2**

(in dcm, sweep rate 50 mV/s; supporting electrolyte: NBu_4PF_6 (0.1 M); reference SCE)

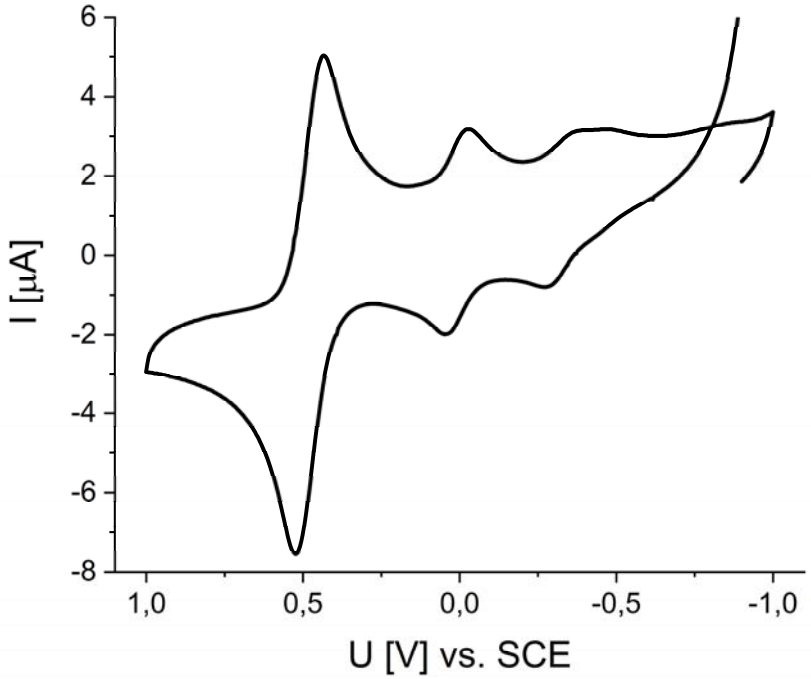

Computational Methods

All quantum chemical density-functional theory (DFT) and time-dependent DFT (TDDFT) calculations were performed with the Turbomole program package [S2] and the ORCA program package,[S3] using the B3LYP functional. Frontier orbitals and their energies (Table 2) were computed using the def2-SVP basis without environment effects. Vertical transitions for neutral and ionic species (Table 3) were computed using the def2-TZVPP basis in combination with the conductor-like screening model (COSMO) employing a dielectric constant of ε=7.5. For all calculations the default convergence criteria were used.

Coordinates of Compound **1a**

	Coordinates [Å]		
Atomic Type	X	Y	Z
N	11.907453	8.953919	3.209956
N	14.141615	9.515233	3.820091
C	12.190475	9.158833	1.920741
C	11.155202	9.073614	0.914705
C	11.481646	9.206781	-0.418738
C	12.85984	9.336854	-0.854328
C	13.824865	9.716231	0.131289
C	13.494107	9.548112	1.503939
C	14.453354	9.734274	2.535004
C	15.80292	10.079133	2.14931
C	16.119164	10.282118	0.818433
C	13.344593	9.134906	-2.181961
C	12.900121	9.124837	4.076874
N	16.39914	10.643818	-5.658401
N	14.73253	9.016849	-6.15714
C	15.993745	10.688517	-4.383146
C	16.57995	11.62035	-3.444919
C	16.216355	11.58282	-2.112621
C	15.30904	10.573758	-1.59965
C	14.516488	9.865632	-2.557339
C	14.922612	9.875038	-3.920344
C	14.296653	9.050374	-4.892402
C	13.232697	8.174415	-4.459559
C	12.801819	8.197813	-3.14733
C	15.111819	10.231291	-0.224915
C	15.757056	9.802654	-6.462015
Cl	16.68717	12.894805	-1.082271
Cl	17.796873	10.372114	0.386558
Cl	10.20678	9.438269	-1.57077
Cl	11.753924	6.923883	-2.614369
Cl	12.607984	7.050656	-5.601616
Cl	17.666361	12.804101	-4.057918
Cl	17.002944	10.120083	3.38276
Cl	9.528528	8.890705	1.443844

C	16.316448	9.643944	-7.882412
F	16.837901	10.781135	-8.34495
F	17.294389	8.720223	-7.869121
F	15.375418	9.233911	-8.735924
C	12.541196	8.863462	5.54457
F	11.943124	9.939768	6.083398
F	11.698848	7.831033	5.643242
F	13.624756	8.588422	6.270587

Final Single Point Energy	−5410.506450395073 E_h	
HOMO:	−0.248239 E_h	−6.7549 eV
LUMO:	−0.156768 E_h	−4.2659 eV

Coordinates of Compound **1b**

	Coordinates [Å]		
Atomic Type	X	Y	Z
N	11.962218	9.106991	3.20227
N	14.23391	9.595679	3.729564
C	12.190378	9.361197	1.910412
C	11.110505	9.349403	0.947814
C	11.391787	9.47785	-0.396807
C	12.758104	9.552197	-0.883635
C	13.768301	9.904607	0.066306
C	13.486348	9.725233	1.448057
C	14.49075	9.866211	2.442216
C	15.825049	10.218822	2.0139
C	16.096412	10.43172	0.674409
C	13.19778	9.310867	-2.221969
C	13.001819	9.206538	4.025847
N	16.34189	10.489663	-5.74448
N	14.623309	8.89718	-6.174405
C	15.90488	10.651208	-4.492474
C	16.504155	11.63086	-3.613403
C	16.144873	11.66821	-2.2813
C	15.220543	10.700429	-1.719671
C	14.390122	9.98377	-2.638645
C	14.797105	9.908243	-3.998783
C	14.150846	9.052001	-4.929136
C	13.02997	8.268835	-4.464747
C	12.600729	8.373203	-3.15396
C	15.054163	10.389961	-0.334635
C	15.700583	9.598765	-6.495317
Cl	16.643086	13.01789	-1.31486
Cl	17.760106	10.519992	0.190894
Cl	10.088534	9.773442	-1.501096

Cl	11.475947	7.186762	-2.579135
Cl	12.337597	7.134588	-5.55747
Cl	17.607458	12.75768	-4.298383
Cl	17.066223	10.251048	3.205989
Cl	9.499263	9.249789	1.542869
C	16.338253	9.324524	-7.863437
F	16.536932	10.480794	-8.534969
F	15.551049	8.528025	-8.608814
C	12.724277	8.810155	5.483115
F	12.038084	7.644741	5.514806
F	13.879662	8.638443	6.150676
C	17.720069	8.617242	-7.718111
F	18.649908	9.465083	-7.283658
F	17.61913	7.609947	-6.837338
F	18.10954	8.115046	-8.887207
C	11.879089	9.857855	6.26133
F	12.373594	11.087091	6.059948
F	10.613227	9.843176	5.851231
F	11.908982	9.589653	7.566061

Final Single Point Energy	−5885.530526412433 E_h	
HOMO:	− 0.248939 E_h	− 6.7740 eV
LUMO:	− 0.157456 E_h	− 4.2846 eV

Coordinates of Compound **1c**

Atomic Type	Coordinates [Å] X	Y	Z
N	11.722515	9.208246	2.983745
N	13.970911	9.739526	3.564837
C	11.974243	9.479764	1.699567
C	10.915925	9.472482	0.711952
C	11.226244	9.621794	-0.623983
C	12.603282	9.692567	-1.082419
C	13.592243	10.039763	-0.10841
C	13.276401	9.860101	1.2666
C	14.254856	10.011179	2.283893
C	15.598074	10.365624	1.890632
C	15.90598	10.563421	0.55727
C	13.070367	9.448218	-2.410913
C	12.74207	9.323221	3.831043
N	16.331158	10.553907	-5.856875
N	14.582698	9.005792	-6.327578
C	15.863545	10.729488	-4.616423
C	16.455763	11.702743	-3.72466
C	16.052116	11.762496	-2.405905

C	15.097743	10.813459	-1.86207
C	14.283427	10.102324	-2.799578
C	14.726319	10.013653	-4.148543
C	14.08541	9.169884	-5.093898
C	12.937047	8.410981	-4.658923
C	12.479232	8.521862	-3.35886
C	14.890643	10.516651	-0.479246
C	15.683028	9.683478	-6.624549
Cl	16.532924	13.120554	-1.442248
Cl	17.583394	10.635357	0.121846
Cl	9.949604	9.948415	-1.75051
Cl	11.319664	7.354101	-2.816546
Cl	12.247432	7.295444	-5.772065
Cl	17.60467	12.801706	-4.38007
Cl	16.80468	10.406166	3.117169
Cl	9.291372	9.361142	1.267658
C	16.31836	9.374023	-7.989774
F	16.973739	10.456839	-8.458366
F	15.376772	9.02205	-8.887474
C	12.469957	8.888459	5.280529
F	11.689341	7.78225	5.265635
F	13.625584	8.578762	5.894831
C	17.325744	8.184964	-7.868897
F	18.114671	8.379429	-6.790808
F	16.615127	7.056702	-7.682125
C	11.765672	9.986753	6.135702
F	10.816515	10.592262	5.394434
F	12.686475	10.907032	6.486252
C	18.27302	7.96287	-9.079884
F	19.146481	8.96182	-9.177879
F	18.949226	6.826732	-8.892583
F	17.580943	7.867045	-10.215434
C	11.079119	9.479158	7.43764
F	10.686031	10.539879	8.145398
F	10.009774	8.741584	7.153294
F	11.919529	8.754528	8.178265

Final Single Point Energy	−6360.553934316494E_h	
HOMO:	− 0.249303 E_h	− 6.7839 eV
LUMO:	− 0.157419 E_h	− 4.2836 eV

Computation of vertical excitation energies of neutral, mono- and dianionic compounds:
Level of Theory: B3LYP/TZVPP

Table SI. Absorption properties and computed frontier orbital energies of neutral, monoanions and dianions of 1 and 2.

	λ_{Abs}[a] [nm]	$\lambda_{Abs,DFT}$[b,c] [nm]	E_{HOMO}[b] [eV]	E_{LUMO}[b] [eV]	Excitation character[b]
1c	501	533 (0.62)	−6.61	−4.08	H→L (98%)
1c$^{\bullet-}$	702	661 (0.53)	−4.21 (α) −5.41 (β)	−1.82 (α) −3.13 (β)	$H_\alpha \rightarrow L_\alpha$ (55%) $H_\beta \rightarrow L_\beta$ (39%)
1c^{2-}	607	574 (0.47)	−3.27	−0.77	H→L (98%)
2	508	543 (0.63)	−6.60	−4.09	H→L (98%)
2$^{\bullet-}$	699	667 (0.52)	−4.24 (α) −5.43 (β)	−1.85 (α) −3.16 (β)	$H_\alpha \rightarrow L_\alpha$ (54%) $H_\beta \rightarrow L_\beta$ (40%)
2^{2-}	613	581 (0.43)	−3.31	−0.81	H→L (98%)

[a] Measured in THF. [b] Computed at TDDFT/B3LYP-TZVPP level of theory employing the COSMO model (ε = 7.5).[c] Oscillator strength in parentheses. Note that using COSMO leads to slightly different orbital energies in Table 2 compared to Table 3, since in the former COSMO is not used.

Coordinates of Compound **1c**

Atomic Type	Coordinates [Å] X	Y	Z
N	11.5451414	9.0937431	2.9886715
N	13.780111	9.4892722	3.7083778
C	11.936826	9.1264673	1.7111301
C	10.9755203	9.0210529	0.6479545
C	11.3947132	9.0102446	-0.6571159
C	12.7950175	9.0473114	-1.0017699
C	13.7109448	9.4071377	0.0235006
C	13.2878885	9.3544794	1.3693378
C	14.1935253	9.5366638	2.437925
C	15.5880366	9.6926674	2.1258089
C	15.9897915	9.8031277	0.8200544
C	13.3450979	8.8193083	-2.2905389
C	12.4890043	9.2709699	3.8977217
N	16.3792357	10.5196914	-5.6394335
N	14.7176878	8.9223659	-6.237904
C	16.0061878	10.4471807	-4.3582406
C	16.6171228	11.2921935	-3.3693263
C	16.2571114	11.1770836	-2.0518657

C	15.3112785	10.1811024	-1.6110382
C	14.5315183	9.5340629	-2.6075916
C	14.9454601	9.6065492	-3.9552184
C	14.3177017	8.8438649	-4.9645709
C	13.2898306	7.9181769	-4.5745453
C	12.8443513	7.8951688	-3.2785148
C	15.0380107	9.8264598	-0.2640057
C	15.7097164	9.75986	-6.4903237
Cl	16.7802178	12.3890673	-0.9363246
Cl	17.6751455	9.6929347	0.452334
Cl	10.2177808	9.1783772	-1.9118372
Cl	11.8272818	6.594158	-2.7684323
Cl	12.7167377	6.8074719	-5.7534292
Cl	17.7248928	12.489831	-3.9078544
Cl	16.7138941	9.6436887	3.4228059
Cl	9.3094904	9.0011138	1.0682103
C	16.1497482	9.8570192	-7.9565152
F	16.6104053	11.1029875	-8.221018
F	15.0994486	9.6193011	-8.7768454
C	12.0218278	9.2476878	5.358659
F	10.9317393	8.454887	5.488124
F	12.995978	8.748641	6.1552654
C	17.2778731	8.8373257	-8.3123529
F	18.3056241	9.0090664	-7.4521618
F	16.7891827	7.5882194	-8.1542748
C	11.6496177	10.6714411	5.8837542
F	10.7262511	11.2083733	5.0559657
F	12.7569597	11.4434672	5.8510188
C	17.8670087	8.9274696	-9.7555881
F	18.4670783	10.1016006	-9.9574751
F	18.7756117	7.95744	-9.9093606
F	16.9145144	8.7635905	-10.6753132
C	11.0725956	10.7547897	7.3321542
F	10.8724499	12.0419142	7.6390314
F	9.9063515	10.11408	7.4250362
F	11.9245222	10.2365001	8.2186406

Final Single Point Energy −6364.9238222770 E_h

Coordinates of Compound **1**$^-$

Atomic Type	Coordinates [Å] X	Y	Z
N	12.1560504	9.3880035	3.1465061
N	14.4478328	9.3594331	3.8228277
C	12.5247438	9.4339618	1.8470786
C	11.5623336	9.537621	0.8098556

C	11.9590869	9.5048506	-0.5190969
C	13.3182845	9.3314235	-0.8920221
C	14.2941327	9.5007886	0.1306926
C	13.8940303	9.4471956	1.4831014
C	14.8455032	9.4043157	2.5326058
C	16.2187279	9.3480421	2.1802118
C	16.6070819	9.4912527	0.8566278
C	13.8207739	9.0520978	-2.2169821
C	13.1416657	9.3608865	4.0245193
N	17.0236743	10.4300679	-5.5872708
N	15.1729861	9.046555	-6.1966846
C	16.6431383	10.3940971	-4.2906407
C	17.3398159	11.1266135	-3.2960764
C	16.9904211	10.9973894	-1.9598452
C	15.9581367	10.1196432	-1.5368955
C	15.0879165	9.6134379	-2.5433188
C	15.4932723	9.6668598	-3.8941219
C	14.767152	8.9946604	-4.9087134
C	13.648708	8.2154276	-4.5173078
C	13.2065464	8.2352846	-3.2024195
C	15.6650987	9.7257053	-0.1795467
C	16.2657446	9.7519716	-6.4288956
Cl	17.7294613	12.0675046	-0.8080182
Cl	18.272264	9.2057326	0.4513425
Cl	10.7742389	9.8566008	-1.7402007
Cl	11.9800789	7.098902	-2.7305977
Cl	12.8929367	7.2172688	-5.7121734
Cl	18.5977625	12.2011385	-3.8041559
Cl	17.371797	9.0568922	3.4374234
Cl	9.9030901	9.7479199	1.2557492
C	16.7080699	9.7928872	-7.8955342
F	18.0218253	10.10737	-7.997273
F	16.5429717	8.568312	-8.4651196
C	12.7149819	9.3068265	5.4970626
F	13.5660302	10.0368692	6.2633972
F	11.4750906	9.8314841	5.6566111
C	15.9266503	10.783633	-8.8200484
F	14.6336271	10.4028787	-8.8857838
F	16.4563042	10.6993626	-10.0638674
C	12.6906185	7.8542534	6.0706913
F	13.9476963	7.3620988	6.0739244
F	11.9282051	7.0802621	5.264997
C	15.9417545	12.2889778	-8.4207077
F	15.2927766	12.9911539	-9.358367
F	15.3203669	12.4764801	-7.2527279
F	17.1867513	12.7579232	-8.32984
C	12.1310359	7.6860802	7.5186656

F	12.8072169	8.440393	8.3888901
F	10.8376669	8.0088173	7.5813204
F	12.2595721	6.4034816	7.8844597

Final Single Point Energy −6365.0752330530 E_h

Coordinates of Compound $\mathbf{1}^{2-}$

Atomic Type	Coordinates [Å] X	Y	Z
N	12.1205439	9.4707061	3.1665068
N	14.4154162	9.3158404	3.8483013
C	12.4980265	9.5390192	1.8528515
C	11.5689484	9.7153751	0.8183652
C	11.9752196	9.6615531	-0.5256002
C	13.3050554	9.4187382	-0.8896798
C	14.2795282	9.5312146	0.1458485
C	13.8734678	9.4776119	1.4959583
C	14.8261988	9.3564667	2.5451477
C	16.1748499	9.2342933	2.1835807
C	16.5751776	9.3984587	0.8473723
C	13.8150539	9.0969793	-2.226676
C	13.1096804	9.3745039	4.0325731
N	17.0638789	10.4131951	-5.6074387
N	15.1962111	9.0374122	-6.2206802
C	16.6691214	10.3958433	-4.2982327
C	17.3497173	11.1130077	-3.3047921
C	16.9952748	10.9734714	-1.9528249
C	15.9663155	10.1189222	-1.5400019
C	15.0957232	9.6305606	-2.5586193
C	15.5089306	9.6718905	-3.9068987
C	14.7803361	8.9888219	-4.9195801
C	13.6668971	8.2370819	-4.5197088
C	13.2039709	8.2909847	-3.1946625
C	15.6606887	9.6963957	-0.1698167
C	16.295119	9.7354811	-6.436766
Cl	17.8006805	11.9957191	-0.7885255
Cl	18.2502853	9.0983828	0.4558108
Cl	10.7873918	10.028417	-1.751837
Cl	11.9021466	7.2181967	-2.7435823
Cl	12.8756009	7.241473	-5.7115767
Cl	18.648247	12.1684742	-3.7924034
Cl	17.3336142	8.8774849	3.4358443
Cl	9.9014133	9.9928477	1.2455697
C	16.7312111	9.7794297	-7.9053387
F	18.0383487	10.1245714	-8.0250877

F	16.595337	8.5498769	-8.4812047
C	12.6897118	9.2942286	5.5058741
F	13.4483173	10.1311702	6.2681477
F	11.3955039	9.671649	5.6735427
C	15.9263375	10.7489385	-8.8310667
F	14.6528779	10.3169651	-8.9421055
F	16.4873095	10.7144802	-10.067626
C	12.8337435	7.8608764	6.1127108
F	14.1382805	7.5776126	6.3032832
F	12.3212021	6.958425	5.2425317
C	15.8660518	12.246288	-8.408112
F	15.2226896	12.938128	-9.3616237
F	15.1964412	12.396984	-7.2638137
F	17.0871682	12.7652396	-8.2697244
C	12.1159932	7.6210145	7.4793745
F	12.4561774	8.5546367	8.3742257
F	10.78793	7.6187536	7.3446684
F	12.4843383	6.4249971	7.9618226

Final Single Point Energy −6365.1935426920 E_h

Coordinates of Compound **2**

Atomic Type	Coordinates [Å] X	Y	Z
N	11.8963114	8.9342169	3.2022225
N	14.0978173	9.5910505	3.8243954
C	12.2273264	8.9954767	1.908599
C	11.2445995	8.7666774	0.8852519
C	11.6151022	8.7714451	-0.4332272
C	12.9915276	8.9481431	-0.8302527
C	13.8966255	9.4353344	0.1499047
C	13.5320184	9.3667257	1.511491
C	14.4546942	9.6683121	2.5387392
C	15.8091967	9.9739722	2.1684683
C	16.1466542	10.0982587	0.8470184
C	13.5211515	8.7381509	-2.1303038
C	12.8510576	9.2254478	4.0692767
N	16.2578605	10.6275332	-5.6293976
N	14.7640861	8.8400042	-6.1187239
C	15.9253925	10.5716358	-4.3362513
C	16.4612908	11.5182772	-3.397425
C	16.1523319	11.4139915	-2.067409
C	15.3414314	10.3316165	-1.5634923
C	14.6090462	9.567949	-2.511157

C	14.9739272	9.6350116	-3.8727201
C	14.4069278	8.766417	-4.8326116
C	13.5009838	7.7484087	-4.3769135
C	13.0988628	7.7254693	-3.0679746
C	15.1572331	9.9897097	-0.1983994
C	15.654639	9.7661262	-6.4306033
Cl	16.5509564	12.7115436	-0.9966091
Cl	17.8148935	10.1691795	0.3976755
Cl	10.3968383	8.7852617	-1.6601916
Cl	12.2489172	6.3468682	-2.462796
C	16.0498496	9.8396191	-7.9102981
F	16.4171769	11.1024486	-8.232996
F	14.9973711	9.5014246	-8.6913844
C	12.4603564	9.1373818	5.5497615
F	11.508104	8.1912029	5.7246255
F	13.5356523	8.7876976	6.2941085
C	17.2362407	8.8851678	-8.2601678
F	18.2519347	9.1207862	-7.3997021
F	16.8231352	7.6102895	-8.0977436
C	11.9071027	10.4869061	6.106322
F	12.852399	11.4383943	5.9462795
Br	17.5035159	12.9342286	-4.0768716
Br	12.9801104	6.4212239	-5.6100153
Br	9.4493498	8.5604457	1.4225435
Br	17.0898172	10.0941154	3.5466588
F	10.819279	10.8361058	5.3860411
C	17.8210349	9.0070564	-9.702616
F	18.392271	10.197541	-9.8905727
F	18.7525218	8.0614335	-9.8696538
F	16.8706971	8.8321446	-10.6229852
C	11.488868	10.5001887	7.6104947
F	11.0486562	11.7251777	7.9216557
F	10.5077444	9.6268194	7.844226
F	12.5241225	10.2109163	8.4007104

Final Single Point Energy −14820.4412954400 E_h

Coordinates of Compound **2**$^-$

Atomic Type	Coordinates [Å] X	Y	Z
N	12.1656274	9.4208884	3.1536094
N	14.4557595	9.3697899	3.8303508

C	12.5326249	9.4809485	1.855083
C	11.5725926	9.6048288	0.8179245
C	11.9688054	9.5712901	-0.5097572
C	13.3265384	9.3778517	-0.8801858
C	14.3040172	9.5382666	0.1413386
C	13.9037798	9.4838279	1.493199
C	14.8570865	9.4248453	2.5417278
C	16.2293256	9.3603508	2.1865152
C	16.6180077	9.5037719	0.8636733
C	13.8258178	9.0841827	-2.2027195
C	13.1498452	9.3743805	4.0313513
N	17.0322173	10.417242	-5.5830037
N	15.1725237	9.0426951	-6.1805694
C	16.6551598	10.3937317	-4.2853767
C	17.3546971	11.129246	-3.2946862
C	17.005409	11.0110741	-1.9582614
C	15.9700493	10.1383116	-1.5302737
C	15.0966018	9.63245	-2.5332605
C	15.5007661	9.6741459	-3.8843313
C	14.7672827	8.9983456	-4.8928673
C	13.6447611	8.2287839	-4.4935849
C	13.2043439	8.2614939	-3.1796506
C	15.6759681	9.7500051	-0.1708289
C	16.2687039	9.7396333	-6.4194587
Cl	17.7382918	12.0794426	-0.8004853
Cl	18.2768419	9.2070655	0.4394577
Cl	10.802928	9.9396332	-1.7444307
Cl	11.9717016	7.1434212	-2.6800442
C	16.7059876	9.7695719	-7.8879025
F	18.0161463	10.0948567	-7.9976253
F	16.5495949	8.5375698	-8.4441528
C	12.7217925	9.2891288	5.5015226
F	13.5533899	10.0266755	6.2813268
F	11.4692598	9.7811007	5.6674057
C	15.9119316	10.7436318	-8.8194785
F	14.6233788	10.3482427	-8.8817785
F	16.4419463	10.6556752	-10.0629257
C	12.7313335	7.8259975	6.0503931
F	14.0077196	7.3974505	6.1361843
F	12.067794	7.0271008	5.1827333
C	15.9109196	12.2518023	-8.4310443
F	15.2539877	12.9404213	-9.3730328
F	15.2880979	12.4403044	-7.2637767
F	17.1507182	12.734792	-8.343669
C	12.0769852	7.6112024	7.4518705
F	12.5932946	8.4455865	8.3580878
F	10.7556361	7.7915547	7.4038353

F	12.3125617	6.3546063	7.8520252
Br	12.8137695	7.1338672	-5.800753
Br	18.737146	12.2946617	-3.8683106
Br	17.4846765	9.0245273	3.5686712
Br	9.7596322	9.8562722	1.3169456

Final Single Point Energy −14820.5932569800 E_h

Coordinates of Compound **2^{2-}**

Atomic Type	Coordinates [Å] X	Y	Z
N	12.1142651	9.4722836	3.1713636
N	14.4095472	9.3342078	3.8510244
C	12.4882212	9.5562297	1.8588492
C	11.5599329	9.7340667	0.8233053
C	11.9658571	9.6850052	-0.5201145
C	13.2973791	9.4459416	-0.8819903
C	14.270533	9.5661229	0.1529649
C	13.8655829	9.5061063	1.5024331
C	14.8218224	9.3872072	2.5502335
C	16.1710794	9.2784728	2.1854108
C	16.5691023	9.4493768	0.8502251
C	13.8105257	9.1185146	-2.2168544
C	13.1038516	9.3765906	4.0366657
N	17.0596337	10.4223149	-5.5990096
N	15.2069412	9.0248886	-6.2031868
C	16.6591663	10.4226315	-4.2924916
C	17.3241881	11.1610036	-3.3033751
C	16.9675159	11.0315527	-1.9517898
C	15.9495031	10.1649961	-1.5358659
C	15.0864359	9.6597198	-2.5516759
C	15.5036701	9.690238	-3.8983393
C	14.7839867	8.9869225	-4.905142
C	13.6755871	8.2309966	-4.4983615
C	13.2082534	8.2947414	-3.1760322
C	15.6491637	9.7429986	-0.1639685
C	16.3018817	9.7268856	-6.4234084
Cl	17.7451803	12.0688303	-0.7818577
Cl	18.2428792	9.1674042	0.4399307
Cl	10.7893423	10.0465022	-1.7588544

Cl	11.9156652	7.2212482	-2.7007072
C	16.7483873	9.7504754	-7.889404
F	18.055707	10.0963169	-8.0039678
F	16.6186869	8.5126473	-8.4481076
C	12.6847383	9.2681362	5.5082834
F	13.4489393	10.0833816	6.287489
F	11.3930239	9.6491724	5.684747
C	15.9482615	10.7046738	-8.8344853
F	14.6750591	10.2714741	-8.9431564
F	16.5145317	10.6483606	-10.0677167
C	12.8224352	7.8200993	6.0808795
F	14.1274153	7.51429	6.2301232
F	12.2739184	6.9450601	5.2045826
C	15.8873712	12.2090521	-8.4373482
F	15.2487328	12.8848847	-9.405302
F	15.2124997	12.3794204	-7.2988182
F	17.1080695	12.7294762	-8.3022143
C	12.1399459	7.5579295	7.4606889
F	12.5488209	8.4426464	8.3758951
F	10.8091792	7.6139373	7.3728254
F	12.474559	6.3306617	7.8860774
Br	12.8307504	7.1233925	-5.8028748
Br	18.7276109	12.3295191	-3.8575407
Br	17.4340919	8.8897149	3.5625521
Br	9.7363459	10.029821	1.3044181

Final Single Point Energy −14820.7127448500 E_h

TFT Fabrication Process

Organic n-channel thin-film transistors were fabricated on 125-µm-thick flexible polyethylene naphthalate substrates (Teonex® Q65 PEN; kindly provided by William A. MacDonald, DuPont Teijin Films, Wilton, U.K.). The TFTs were fabricated in the bottom-gate, top-contact (inverted staggered) device structure. In the first step, a 30-nm-thick layer of aluminum was deposited by thermal evaporation in vacuum through a polyimide shadow mask (CADiLAC Laser, Hilpoltstein, Germany). The substrate was then briefly exposed to an oxygen plasma to increase the thickness of the native aluminum oxide (AlO_x) layer to about 3.6 nm and then immersed into a solution of *n*-tetradecylphosphonic acid (PCI Synthesis, Newburyport, MA, U.S.A.) in 2-propanol to allow the formation of a self-assembled monolayer (SAM) on the plasma-oxidized aluminum surface. The hybrid AlO_x/SAM gate dielectric has a thickness of 5.4 nm and a unit-area capacitance of 700 nF/cm^2. Next, a 30-nm-thick layer of the perhalogenated TAPP derivative **1c** was deposited as the organic semiconductor by thermal sublimation in vacuum through another shadow mask. During the semiconductor deposition, the substrate was held at a temperature of 110 °C. Finally, a 30-nm-thick layer of gold was deposited by thermal evaporation in vacuum through a shadow mask to define the source and drain contacts. Mask alignment was performed manually using an optical microscope. The TFTs have a channel length of 20 µm and a channel width of 100 µm. All electrical measurements were performed in ambient air at room temperature.[S4]

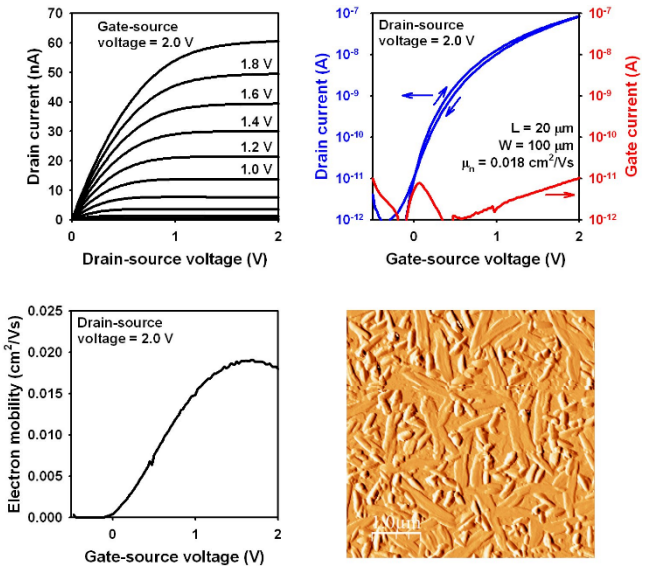

Electrical characteristics of n-channel organic thin-film transistors with a vacuum-deposited layer of 1 as the semiconductor measured in ambient air, and AFM image of the organic-semiconductor surface.

Crystal Structures of Compounds

X-ray Crystal Structure Determinations

Crystal data and details of the structure determinations are compiled in Table S1. Full shells of intensity data were collected at low temperature with an Agilent Technologies Supernova-E CCD diffractometer (Mo- or Cu-K_α radiation, microfocus X-ray tubes, multilayer mirror optics). Detector frames (typically ω-, occasionally φ-scans, scan width 0.5 or 1°) were integrated by profile fitting.[S5,S6] Data were corrected for air and detector absorption, Lorentz and polarization effects[S6] and scaled essentially by application of appropriate spherical harmonic functions.[S7,S8] Absorption by the crystal was treated with a semiempirical multiscan method (as part of the scaling process) and augmented by a spherical correction,[S7,S8] or numerically (Gaussian grid).[S8,S9] An illumination correction was performed as part of the numerical absorption correction.[S8]

The structures were solved by ab initio dual space methods involving difference Fourier syntheses (VLD procedure, compound **1c**)[S10] or by the heavy atom method combined with structure expansion by direct methods applied to difference structure factors (compound **2**)[S11] and refined by full-matrix least squares methods based on F^2 against all unique reflections.[S12] All atoms were given anisotropic displacement parameters. A split atom model was used to refine disorder in compound **1c**. Suitable geometry and adp restraints/constraints were applied to ensure stability of the refinement.[S13]

CCDC 1980430 and 1980431 contains the supplementary crystallographic data for this paper. These data can be obtained free of charge from the Cambridge Crystallographic Data Centre's and FIZ Karlsruhe's joint Access Service via https://www.ccdc.cam.ac.uk/structures/?.

Compound **1c**

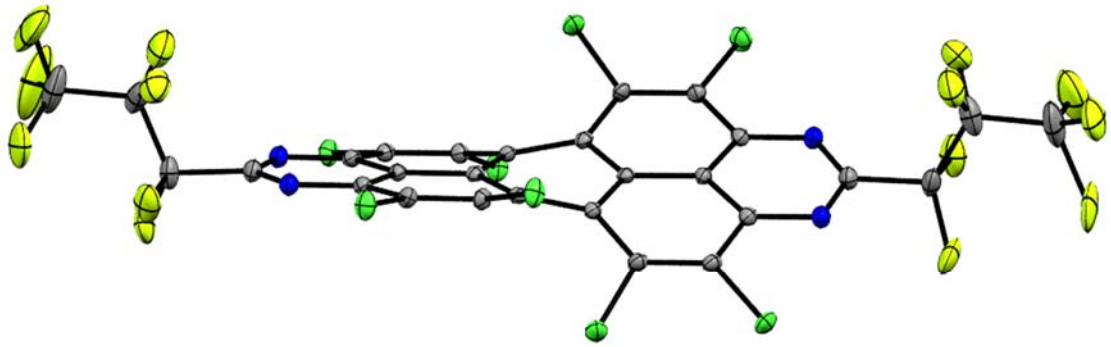

Figure S1. Ortep view (50% probability level) of **1c** (C = grey, N = blue, F = yellow, Cl = green). Only one set of the disordered $N_2CC_3F_7$ moiety is shown.

Compound **2**

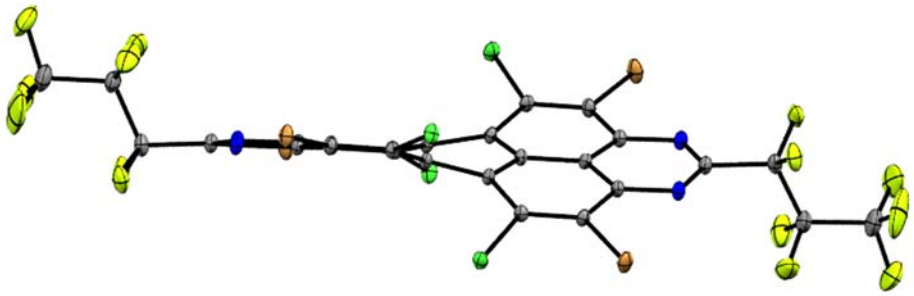

Figure S2. Ortep view (50% probability level) of **2** (C = grey, N = blue, F = yellow, Cl = green, Br = brown). The molecule has crystallographic C_2 symmetry.

Table S1. Details of the crystal structure determinations of compounds **1c** and **2**.

	1c	**2**
formula	$C_{28}Cl_8F_{14}N_4$	$C_{28}Br_4Cl_4F_{14}N_4$
crystal system	monoclinic	monoclinic
space group	*P* $2_1/c$	*I* 2/*a*
a /Å	14.84918(15)	13.3677(2)
b /Å	15.60923(11)	15.88433(19)
c /Å	13.41390(17)	16.0414(2)
β /°	102.9467(11)	97.5267(15)
V /Å^3	3030.09(5)	3376.83(9)
Z	4	4
M_r	941.92	1119.76
F_{000}	1832	2120
d_c /Mgm^{-3}	2.065	2.203
μ /mm^{-1}	7.934	5.192
max., min. transmission factors	1.0000, 0.4254 [a]	0.897, 0.705 [b]
X-radiation, λ /Å	Cu K_α, 1.54184	Mo K_α, 0.71073
data collect. temperat. /K	120(1)	120(1)
θ range /°	3.1 to 71.2	2.6 to 32.4
index ranges *h*,*k*,*l*	-18 ... 18, -19 ... 19, -16 ... 13	-19 ... 20, -23 ... 23, -23 ... 23
reflections measured	169426	35077
unique [R_{int}]	5817 [0.0768]	5813 [0.0321]
observed ($I \geq 2\sigma(I)$)	5180	5163
data / restraints /parameters	5817 / 339 / 599	5813 / 72 / 244
GooF on F^2	1.072	1.066
R indices ($F>4\sigma(F)$) $R(F)$, $wR(F^2)$	0.0365, 0.0756	0.0292, 0.0679
R indices (all data) $R(F)$, $wR(F^2)$	0.0442, 0.0787	0.0357, 0.0702
largest residual peaks /eÅ^{-3}	0.451, -0.664	1.012, -0.450
CCDC deposition number	1980430	1980431

[a] semiempirical absorption correction. [b] numerical absorption correction.

References

[S1] Günther, B. A. R.; Höfener, S.; Zschieschang, U.; Wadepohl, H.; Klauk, H.; Gade, L. H. *Chem. – A Eur. J.* **2019**, *25*, 14669–14678.

[S2] Turbomole, a development of University of Karlsruhe and Forschungszentrum Karlsruhe GmbH, 1989–2007, TURBOMOLE GmbH, since 2007; available from http://www.turbomole.com.

[S3] ORCA, a development of the Max Planck Institute for Chemical Energy Conversion, Mülheim a.d. Ruhr; available from https://orcafor-um.cec.mpg.de/; Neese, F. WIREsComput. Mol.Sci. 2012, 2, 73.

[S4] Geib, S.; Zschieschang, U.; Gsänger, M.; Stolte, M.; Würthner, F.; Wadepohl, H.; Klauk, H.; Gade, L. H. *Adv. Funct. Mater.* **2013**, *23*, 3866–3874.

[S5] Kabsch, K. in: Rossmann, M. G.; Arnold, E.; (eds.) *"International Tables for Crystallography" Vol. F*, Ch. 11.3, Kluwer Academic Publishers, Dordrecht, The Netherlands, **2001**.

[S6] *CrysAlisPro*, Agilent Technologies UK Ltd., Oxford, UK **2011**-**2014** and Rigaku Oxford Diffraction, Rigaku Polska Sp.z o.o., Wrocław, Poland **2015**-**2019**.

[S7] Blessing, R. H. *Acta Cryst.* **1995**, *A51*, 33.

[S8] *SCALE3 ABSPACK, CrysAlisPro*, Agilent Technologies UK Ltd., Oxford, UK **2011**-**2014** and Rigaku Oxford Diffraction, Rigaku Polska Sp.z o.o., Wrocław, Poland **2015**-**2019**.

[S9] Busing, W. R.; Levy, H. A. *Acta Cryst.* **1957**, *10*, 180.

[S10] (a) Burla, M. C.; Caliandro, R.; Carrozzini, B.; Cascarano, G. L.; Cuocci, C.; Giacovazzo, C.; Mallamo, M.; Mazzone, A.; Polidori, G. *SIR2014*, CNR IC, Bari, Italy, **2014**; (b) Burla, M. C.; Caliandro, R.; Carrozzini, B.; Cascarano, G. L.; Cuocci, C.; Giacovazzo, C.; Mallamo, M.; Mazzone, A.; Polidori, G. *J. Appl. Cryst.* **2015**, *48*, 306.

[S11] (a) Beurskens, P. T.; Beurskens, G.; de Gelder, R.; Smits, J. M. M.; Garcia-Granda, S.; Gould, R. O. *DIRDIF-2008*, Radboud University Nijmegen, The Netherlands, **2008**; (b) Beurskens, P. T. in: Sheldrick, G. M.; Krüger, C.; Goddard, R. (eds.), *Crystallographic Computing 3*, Clarendon Press, Oxford, UK, **1985**, p. 216.

[S12] (a) Sheldrick, G. M. *SHELXL-20xx*, University of Göttingen and Bruker AXS GmbH, Karlsruhe, Germany **2012**-**2018**; (b) Robinson, W.; Sheldrick, G. M. in: Isaaks, N. W.; Taylor, M. R. (eds.) *„Crystallographic Computing 4"*, Ch. 22, IUCr and Oxford University Press, Oxford, UK, **1988**; (c) Sheldrick, G. M.; *Acta Cryst.* **2008**, *A64*, 112; (d) Sheldrick, G. M. *Acta Cryst.* **2015**, *C71*, 3.

[S13] (a) Rollett, J. S. in: Ahmed, F. R.; Hall, S. R.; Huber, C. P.; (eds.) *„Crystallographic Computing"* p.167, Munksgaard, Copenhagen, Denmark, **1970**; (b) Watkin, D. in: Isaaks, N. W.; Taylor, M. R. (eds.) *„Crystallographic Computing 4"*, Ch. 8, IUCr and Oxford University Press, Oxford, UK, **1988**; (c) Müller, P.; Herbst-Irmer, R.; Spek, A. L.; Schneider, T. R.; Sawaya, M. R. in: P. Müller (ed.) *"Crystal Structure Refinement"*, Ch. 5, Oxford University Press, Oxford, UK, **2006**; (d) Watkin, D. *J. Appl. Cryst.* **2008**, *41*, 491.